Journal of Volcanology and Geothermal Research 431 (2022) 107652

Contents lists available at ScienceDirect

Journal of Volcanology and Geothermal Research

journal homepage: www.journals.elsevier.com/journal-of-volcanology-and-geothermal-research

The interplay between environmental and magmatic conditions in eruption style transitions within a fissure-aligned monogenetic volcanic system of Auckland, New Zealand

April Foote [a,*], Károly Németh [b,c], Heather Handley [a,d]

[a] Department of Earth and Planetary Sciences, Macquarie University, Sydney, Australia
[b] School of Agriculture and Environment, Massey University, Palmerston North, New Zealand
[c] Institute of Earth Physics and Space Sciences, Sopron, Hungary
[d] Department of Applied Earth Sciences, University of Twente, Enschede, the Netherlands

ARTICLE INFO

Keywords:
Phreatomagmatic
Magmatic
Auckland volcanic field
Wiri Mountain
Tuff ring
Tephra

ABSTRACT

Recent conceptual geological frameworks of continental monogenetic volcanism highlight that the small magma volume eruptions, resulting volcanic geology and edifice architecture in such settings are sensitive to variations in external or environmental conditions. These conditions, along with fluctuations in magma flux, can change rapidly over short time frames and cause dramatic changes in eruption style. Understanding the drivers of transitions in explosive to effusive behaviour within the short timescales of eruptions at individual volcanic centres is essential to accurately assess volcanic hazards in continental monogenetic settings. Wiri Mountain Volcanic Complex is one of the largest and most complex volcanic centres in the active Auckland Volcanic Field. Despite the significant removal of much of the original volcanic deposits, present-day exposures and historical images provide a unique opportunity to examine the growth and evolution of the volcanic complex. Wiri Mountain deposited an initial basal tuff ring (covering an area of approximately 0.67 km^2) by predominantly pyroclastic density currents, followed by at least two smaller tuff rings erupted through the outer flanks of the first, in a transition from phreatomagmatic to Strombolian eruptive style. A 90 m high central scoria cone was then produced within the initial tuff ring, partially capped by lava spatter, clastogenic lava flows and lava flows that mostly covered all tuff rings, the scoria cone, and the surrounding area. A high-resolution stratigraphic study of the well-exposed tuff ring to capping magmatic succession was conducted to determine the changes in eruptive style and their driving forces. The deposit architecture of Wiri Mountain can be described using three volcanic stratigraphic units: a basal unit comprised of tuff, lapilli tuff and tuff breccia deposits, a middle unit comprised of juvenile-rich transitional tuff deposits of black scoria ash and lapilli, red scoria and spatter, and a capping unit comprised of agglutinate and lava flow successions. Most volcanic materials were either fragmented and ejected at near-optimal scaled depth, or the transition between near-optimal and shallower/deeper depths. Wiri Mountain provides a striking example of a fissure eruption likely controlled by a pre-existing tectonic fault that was fed by relatively stable melt sources over a sustained period. We infer that despite eruption within a water-saturated coastal plain, the initial phreatomagmatic phase was overridden by subsequent explosive and effusive magmatic phases through the formation of an increasingly established conduit, thus allowing sustained magma flux and melt supply. The transitions, both gradual and rapid, from an initial phreatomagmatic to subsequent magmatic explosive and effusive phases fit well to the general understanding of eruption style changes over time from other larger and more complex volcanoes of Auckland, and elsewhere worldwide. Wiri Mountain showcases the fine balance between the external and internal conditions that control eruption style variations and govern the formation of complex monogenetic volcanoes.

* Corresponding author.
E-mail address: april.c.foote@gmail.com (A. Foote).

https://doi.org/10.1016/j.jvolgeores.2022.107652
Received 8 December 2021; Received in revised form 26 July 2022; Accepted 21 August 2022
Available online 27 August 2022

1. Introduction

Intraplate continental basaltic volcanic fields (ICBVs), also termed continental monogenetic volcanic fields or dispersed continental volcanic fields, are volcanic regions containing tens to hundreds of dispersed, typically small-volume, short-lived volcanoes that are of great interest in volcanology. Intraplate volcanic fields within continental lithospheric settings are important geological features as their volcanoes, eruptive products and spatial distribution provides vital information of how primary, deep-sourced magma can segregate and find its way to the surface (Brenna et al., 2015a; Hopkins et al., 2020). In contrast to large and long-lived stratovolcanoes, the relatively simple volcanic architecture of individual vents within volcanic provinces affords invaluable insight into the fundamental processes that build volcanoes and the internal and external factors that govern variations in eruptive style and explosivity (Németh and Kereszturi, 2015). The Auckland Volcanic Field (AVF) in New Zealand is among the few hundred documented dispersed continental volcanic provinces worldwide that has been active through the Holocene (Venzke, 2013) and can broadly be defined as a mafic intraplate monogenetic volcanic field (e.g. Allen and Smith, 1994; Sigurdsson, 2015; Hopkins et al., 2020). Monogenetic volcanoes are those created by one eruption or eruptive phase, which can last up to several years (Cas and Wright, 1988; Walker, 1993; Sigurdsson, 2015). The monogenetic nature of volcanism is typically characterised in the way magma reaches the surface from deep source regions through a relatively simple pathway without significant stalling, producing volcanoes characterised by short-lived activity with eruptive volumes significantly smaller than those considered as polygenetic stratovolcanoes (Kereszturi and Németh, 2012).

The volcanic landforms produced in intraplate basaltic continental volcanic provinces vary greatly, as their architecture is dependent on the incidence and location of magma-water interaction, which is in turn influenced by the source of water and its depth, the nature of the host country-rock, and topography (Lorenz, 1986; Cas and Wright, 1988; Kereszturi et al., 2014). Typical volcanic landforms include maars, tuff rings, tuff cones, scoria cones, small shield volcanoes and lava flows (Cas and Wright, 1988; Kereszturi and Németh, 2012). These small-volume eruptions can be driven by either explosive phreatomagmatic or magmatic eruptions, or both, with deposits derived from pyroclastic fall, pyroclastic density currents (pyroclastic flows and pyroclastic surges) and lava flows (Cas and Wright, 1988; Németh and Kósik, 2020). Recent conceptual frameworks of continental monogenetic volcanism demonstrated that due to the small magma volume associated with this type of volcanism, the eruptions and resulting volcanic geology and edifice architecture are very sensitive to variations of the external or environmental conditions acting upon the eruptions, even over a very short time scale, within eruptive pulses and phases (Németh, 2010; Kereszturi et al., 2014; Németh and Kereszturi, 2015). Along with magma flux, these conditions can change rapidly in the short time span of these eruptions, causing dramatic changes to eruption style. Consequently, these small-volume volcanoes commonly display an extreme variety of volcanic deposits that rapidly change both laterally and vertically, as demonstrated explicitly from some iconic locations in recent years, such as Jeju Island in Korea (Sohn and Park, 2005; Sohn et al., 2012; Brenna et al., 2015b), Mt. Gambier in Australia (van Otterloo et al., 2013), Cerro Overo maar in Northern Chile (Ureta et al., 2021), and Tecuitlapa Maar in Mexico (Ort, 2009). Changes in vent location are also not unusual, often with the presence of multiple vents, either concurrent or in succession throughout eruptive activity (e.g. Wohletz and Sheridan, 1983; Ort, 2009; Pedrazzi et al., 2016; Volosín and Risso, 2019). Recognition of the temporal variation of the dominant type of eruption styles (e.g., wet versus dry) of individual monogenetic volcanoes within a volcanic field has been used as a proxy to record regional environmental changes influencing the region's external water abundance (Kereszturi et al., 2011; Kshirsagar et al., 2015; Kshirsagar et al., 2016). The transition(s) in eruptive style from phreatomagmatic to magmatic or vice versa throughout an eruption period is an important factor to document for volcanic provinces, as the resulting hazard implications and volcanic landforms will change dramatically with each transition.

This paper provides a stratigraphic study of the last remaining outcrops of Wiri Mountain volcanic complex (Fig. 1): one of the southernmost volcanic centres in the AVF, the classification of volcanic facies architecture and reconstruction of the eruptive history. Over the last century, quarrying has removed the majority of the volcanic complex (Hayward et al., 2011; Németh et al., 2021), resulting in the exposure of near vent and crater infill deposits. Therefore, despite the near complete removal of the Wiri Mountain scoria cone and most of the tuff rings, the remaining deposits provide a unique opportunity to document a high-resolution stratigraphy. Such a possibility is not a common occurrence in Auckland where urban development has restricted access to many centres and, in some cases, removed them entirely (Gravis et al., 2020; Németh et al., 2021). The well-exposed tuff ring to capping magmatic succession allows us to develop high-resolution documentation of the eruption deposits and related eruption style changes at one of the largest volcanoes of Auckland. In this aspect, this study is locally and globally relevant as it targets a critical question of why and how eruption style changes take place within a narrow window of time and space in a continental monogenetic setting. These questions are essential when assessing volcanic hazards and predicting the potential order and magnitude of events (e.g. Kósik et al., 2016; Hayes et al., 2020; Hopkins et al., 2020).

2. The active Quaternary Auckland Volcanic Field

The city of Auckland and the active AVF share the same location in the North Island of New Zealand (Fig. 1). Auckland hosts 1.6 million people (Stats, 2018) who live in close proximity to 53 monogenetic volcanoes that have formed over the last 193,200 years (Leonard et al., 2017; Hopkins et al., 2020) (Fig. 1). Recent studies correlating tephra deposits with source centres (Bebbington and Cronin, 2011; Green et al., 2014; Kawabata et al., 2016; Hopkins et al., 2017; Peti and Augustinus, 2019) have provided a relative and absolute chronology of volcanic activity in the AVF for the majority of centres (48 of 53), with activity ranging from at least 193.2 ka (Pupuke) (Leonard et al., 2017) to 504 cal. Yrs. BP (Rangitoto 2) (Needham et al., 2011). These studies show clusters of volcanic activity have occurred both temporally and spatially throughout the history of the field, with half of all eruptions occurring between 15 and 35 ka (Hopkins et al., 2017). The AVF represents the youngest intraplate volcanic field in the North Island, predated by Okete, Ngatutura and South Auckland volcanic fields, respectively (Briggs et al., 1994; Smith and Cronin, 2021) (Fig. 1b).

Eruptive styles and products have varied greatly at individual centres in the AVF (Németh et al., 2012). The majority of volcanic centres commenced with phreatomagmatic activity (83%; Kereszturi et al., 2014), determined by the degree of magma-water interaction, followed by either Hawaiian or Strombolian eruptions, effusive activity, or both (Kereszturi et al., 2014) from one or several clustered vents (Searle, 1959; Houghton et al., 1999).

3. Wiri Mountain Volcanic Complex

Wiri Mountain, also known as Matukutūruru or Te Manurewa o Tamapahore in Māori, is one of the southernmost volcanic centres in the AVF (Fig. 1) and is situated in the well-drained coastal region of South Auckland. Historical studies described Wiri Mountain as a tuff ring containing a 90 m-high scoria cone (Searle, 1959; Rout et al., 1993) covered by extensive deposits of vesicular basalt lava flows, well-bedded scoria, agglutinate and lava spatter with a small summit crater on the north-eastern side of the cone (Firth, 1930). An additional small crater dissected the lava flows to the south west of the main scoria cone (Hayward, 2015) (Fig. 3c), and a number of vents over a small area were reported by Searle (1961). Radiocarbon ages from wood charcoal buried

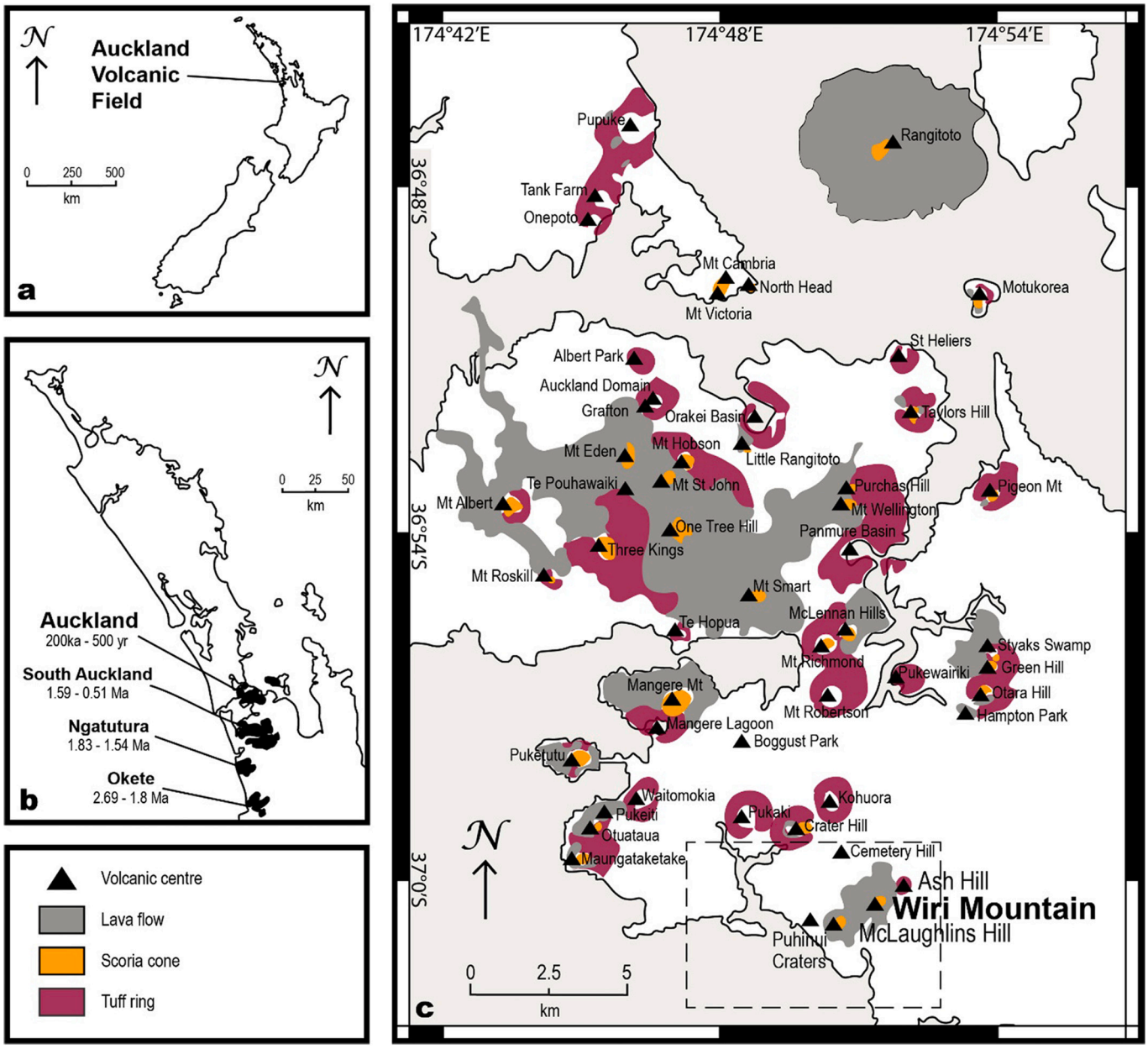

Fig. 1. a) Location of the Auckland Volcanic Field (AVF) in New Zealand, b) Location of the AVF and other intraplate volcanic fields in the North Island, New Zealand, c) Volcanic centres and deposits of the AVF (Briggs et al., 1994; Edbrooke, 2001; Cassidy and Locke, 2010; Hopkins et al., 2017), dashed inset see Fig. 2, scale from GNS (2020).

beneath deposits (Polach et al., 1969; Grant-Taylor and Rafter, 1971), K—Ar (Mochizuki et al., 2004), Ar—Ar and palaeomagnetic (Cassata et al., 2008) dating of volcanic materials provide an age of between 27 and 33 ka for Wiri Mountain (Lindsay et al., 2011; Hopkins et al., 2017).

Wiri sits on the Manurewa Horst, bounded to the north by the Wiri Fault and to the south by the Karaka Fault, both subsurface structures inferred by Kenny et al. (2012) from borehole information and topographic and lithologic offset. The Wiri and Karaka Faults are two of many ENE trending faults that form horst and graben structures in basement and Waitemata Group rocks across the Manukau lowlands and through South Auckland (Berry, 1986; Kenny et al., 2012).

Several other volcanic centres occur near Wiri Mountain, including McLaughlins Hill (also known as Matukutūreia) to the south west and Ash Hill, a 200 m wide tuff ring to the north east (Cassidy and Locke, 2010), the deposits of which have been entirely removed (Fig. 2). The alignment of volcanism in the area is attributed to underlying structural controls such as the inferred Wiri Fault (Von Veh and Németh, 2009; Cassidy and Locke, 2010; Kenny et al., 2012; Kereszturi et al., 2014) (Fig. 2). The concealed Wiri Fault is suggested to have aided magma ascent through basement rocks, with the fractured nature of the underlying Waitemata group rocks facilitating magma ascent (Kenny et al., 2012). Wiri Mountain and Ash Hill are located only 900 m apart, with absolute eruption ages in error of each other at 30.2 ± 4.6 ka and 31.8 ka ± 159 cal yr BP, respectively (Hayward, 2008; Hopkins et al., 2017), indicating their eruptive activity could have been part of the same magmatic episode (Hayward, 2008). The Puhinui Craters are presently undated, however, their aligned nature with the Wiri Fault indicate a potential relationship with fault-aligned volcanism in the area and it has been speculated that they may be related to activity at McLaughlins Hill (Hayward et al., 2012; Hayward, 2015).

There has been limited prior studies of the volcanic stratigraphy, magma ascent and eruption dynamics of Wiri Mountain Volcanic

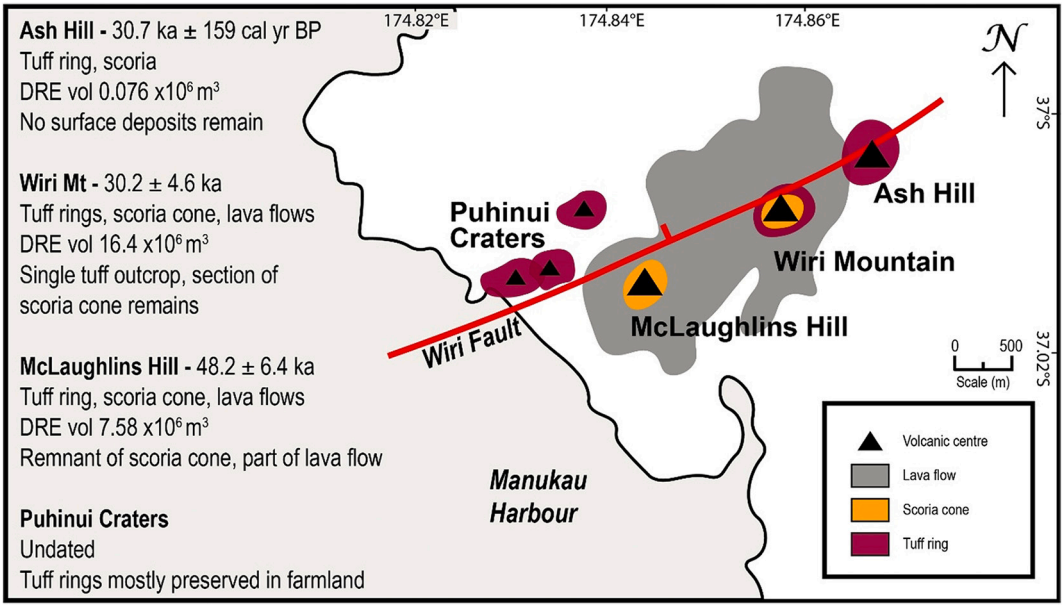

Fig. 2. Temporal and spatial relationships in the southern Auckland Volcanic Field (AVF) between McLaughlins Hill, Puhinui Craters, Wiri Mountain and Ash Hill (Dense Rock Equivalent (DRE) volumes calculated by Kereszturi et al. (2014). Age data is from Cassata et al. (2008), Hayward (2008) and Leonard et al. (2017) using Carbon14 and Argon-Argon dating methods. Geological interpretations are based on field observations and measurements by Hayward (2008), Hayward et al. (2012), Kenny et al. (2012) and Hayward (2015). Map covers inset from Fig. 1, scale from GNS (2020).

Complex. Several lava samples and a single scoria cone sample from the complex were included in a geochemical study of source melting processes across the AVF (McGee et al., 2013). The results suggest that Wiri Mountain was supplied by melting of a fertile, deep garnet-bearing source and the associated incorporation of 2% lithospheric mantle (McGee et al., 2013). Rock composition based on bulk rock chemistry analysis for the samples taken throughout exposures in the Wiri volcanic complex includes nephelinite, basanite and basalt (McGee et al., 2013).

Winstone Aggregates began quarrying activities at Wiri Mountain circa 1920 (Collections, 1922) to supply ballast for nearby rail tracks. Most of the surficial volcanic deposits of Wiri Mountain have since been removed to a current quarried depth of 40 m above sea level (Németh et al., 2021), with the exception of the outcrops included in this study and Wiri Mountain lava cave (Fig. 3c).

Wiri Mountain lava cave is the longest known lava tube in New Zealand at approximately 300 m long (Hayward et al., 2011). It has been identified as internationally significant due to its accessibility and abundance of geological features (Kermode, 1994; Hayward and Crossley, 2014). The cave was deemed vulnerable to destruction due to the nearby quarrying activities and was protected as a scientific reserve by the Department of Conservation in 1990 (DOC, 1990).

4. Materials and methods

4.1. Field observations and sampling

The thickness, colour, grain size, bedding, sorting, grading, and componentry of the deposits were recorded in the field, including the lithic to juvenile ratio and the rock type of larger clasts following White and Houghton (2006). Mixed deposit terms are defined by Fisher (1966) and Schmid (1981). For this study, two types of pyroclasts are defined: 1) juvenile clasts produced directly by magma in the eruption, that can be recycled (involved in more than one explosion and redeposited after their original deposition) during the eruption and 2) lithic clasts obtained through fragmentation of country rocks from the underlying strata (Fisher and Schminke, 1984). Samples were taken from each layer accessible from each outcrop (53 samples) and bulk samples were taken where possible. Samples taken from outcrop were mostly loose and unlithified, and samples that needed to remain stratigraphically intact for thin section had to be treated with care.

4.2. Sample preparation

Loose bulk samples (20 samples) were dried for at least 24 h, and dry sieved using 1 ϕ increments from −5 to 4 ϕ (32 mm - 62.5 μm). Sieved increments were then weighed to define grain size distribution. Loose grains of all samples were classified according to componentry and counted by hand and under the microscope, for each entire individual sieved size range between −5 and 3 ϕ (32 mm - 125 μm). All juvenile clasts (46 clasts) were picked from sieved samples, using both −4 to −5 ϕ (16–32 mm) and − 5 ϕ (32 mm) and above size fractions. Each clast was wrapped in a parafilm wax sheet and weighed in air and water following the Archimedes method. Buoyant clasts were weighed down using a ballast. An area specific Dense Rock Equivalent volume (DRE) was calculated by measuring both clast weight and water displacement of a range of samples taken from non-vesicular, dense lava flow samples from Wiri Mountain. Clast density and vesicularity were then calculated after Houghton and Wilson (1989). Sixteen polished thin sections were created of a range of samples representative of the varying stages of the eruption based on initial observations.

5. Volcanic lithofacies of Wiri Mountain

Two main outcrops remain exposed at Wiri Mountain; a 200 m long outcrop oriented north to south (locality 1) of tuff, lapilli tuff, tuff breccia, scoria rich tuff, and agglutinated spatter and lava, and a 100 m long outcrop oriented west to east (locality 2) consisting of scoria tuff, scoriaceous lapilli and spatter, and agglutinated spatter and lava. A minor lava outcrop is also exposed on the northern outskirts of the quarry (locality 3). The deposit architecture of Wiri Mountain can be described using three volcanic stratigraphic units: 1) a Basal Unit (BU) comprised of tuff, lapilli tuff and tuff breccia deposits, 2) a Middle Unit (MU) comprised of juvenile-rich transitional tuff deposits of black scoria ash and lapilli, red scoria and spatter, and 3) a Capping Unit (CU) comprised of agglutinate and lava flow successions. The deposits represented by these stratigraphic units have been classified into eleven

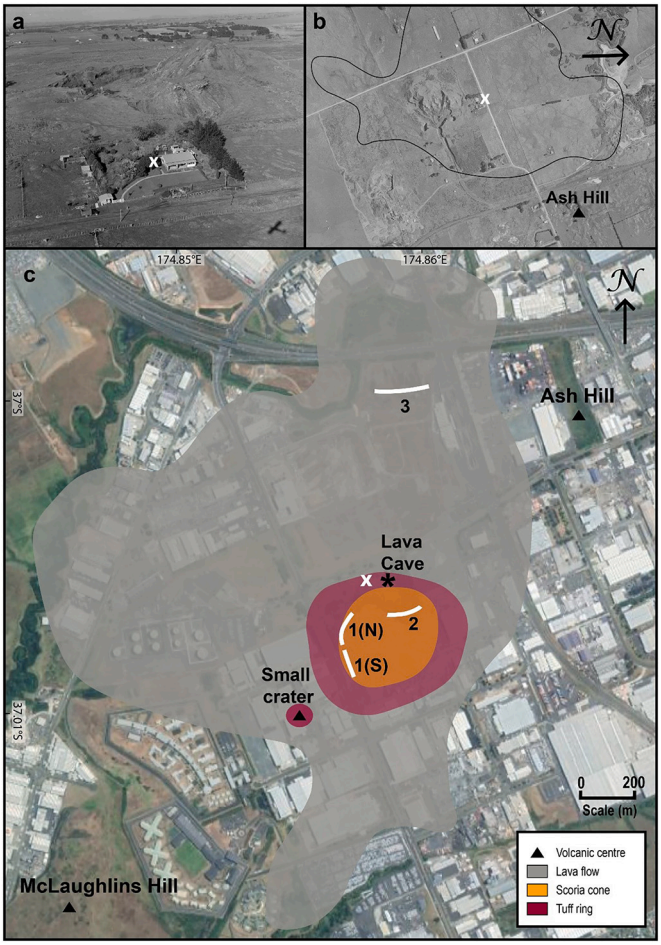

Fig. 3. a) Historic aerial view of Wiri Mountain looking south (Whites Aviation, 1949) (white X shows the location of the historical Rumney Cottage on each panel), b) Historical photo of Wiri Mountain (LGGA, 1925) with outline of lava flow overlain, c) Outcrop locations (white lines) and deposits at Wiri Mountain based on field observations, historical photography and literature (DOC, 1990; Edbrooke, 2001; Hayward, 2015; Hopkins et al., 2020). Satellite image from Google Earth (Google., 2020), scale from GNS (2020).

volcanic lithofacies, classified after Sohn and Chough (1989) and Chough and Sohn (1990) (Table 1), based on the guidelines of lithofacies description proposed by Cas and Wright (1988) and White and Houghton (2006). Detailed unit and facies descriptions and their corresponding interpretations are displayed in Table 2 below.

Table 1
Fragmental volcanic lithofacies classification scheme based on abundance and classification of clasts, grain size and sedimentary structures.

Volcanic lithofacies	Tuff (T)	Lapilli Tuff (LT)	Tuff Breccia (TB)
Lithic rich			
Massive		LT1 (BU)	TB1 (BU)
Thinly bedded		LT2 (BU)	TB2 (BU)
Cross-bedded			TB3 (BU)
Inverse-graded		LT3 (BU)	
Juvenile rich			
Unsorted-massive			
Weakly bedded	ST1 (MU)		
Thinly bedded		LT4 (MU)	
Cross-bedded	ST2 (MU)	SSL (MU)	

Table 2
Volcanic stratigraphic units and associated facies, descriptions, and interpretations.

Volcanic stratigraphic units	Facies	Description	Interpretation
Capping Unit (CU)	SAF	Medium to dark grey, weakly to moderately welded spatter and strongly welded agglutinated spatter rafts of varying vesicularity. Rafts vary, some have increased vesicularity upwards or chilled margins, and many often exhibit linear vesicle distributions alternating between internal horizontal bands of lower or no vesicularity. Larger rafts have developed joints in many directions. Commonly forms lava flows, distal flows have rubbly surfaces with vesicles stretched towards north-east concentrated in bands underneath. 100% juvenile. Thickness not uniform, ranges 1.1–4 m.	Represents transition phase from Strombolian-style explosive eruptions towards Hawaiian-style lava fountaining[5,6,7] and formation of clastogenic lava flows and agglutinates. Weakly to moderately welded spatter caused by pulsing of fountains[5]. Textural features of agglutinated spatter indicate rheomorphism and formation of clastogenic lava (Figs. 5b, c).
Middle Unit (MU)	LT4	Medium to dark grey lapilli tuff predominantly of fine lapilli alternating with thin fine to coarse ash beds and coarse lapilli angular and subrounded to rounded pale grey siltstone lithics, thinly bedded, juvenile-rich. Beds are oriented 200,60. Deposits become orange-brown in colour when scoria spatter and flows are deposited above. Lithic to juvenile ratio ranges 8:92 to 19:81. Thickness ranges 0.6–0.7 m.	Transition phase from phreatomagmatic to magmatic eruptions caused by increase in magma flux and decreasing water interactions[3,4,7]. Pyroclastic fall deposits followed by settling of suspended fines[1,2]. Some recycling of clasts[9] (Figs. 4c, d).
	ST1	Dark brown to dark red scoria tuff predominantly of coarse ash to medium lapilli, with occasional alternating diffuse beds of coarse ash, disorganised, crudely stratified. Coarse lapilli dense subangular juvenile bombs up to 7 cm occur, as well as approximately 2% pale brown subrounded lithics up to 6 cm. Lithic to juvenile ratio ranges 24:76 to 2:98. Thickness not uniform, ranges 0.5–3.5 m.	Strombolian style explosive eruptions with rhythmic variations in fragmentation creating couplets of finer material through a debris filled vent[1,2]. Minor recycling of clasts[9] (Fig. 5a).
	ST2	Dark red to dark purple scoria tuff alternating between coarse and fine beds, some cross bedding, well-defined individual beds, and lenses that are separated	Strombolian style explosive eruptions and ballistic curtain deposits with distinct rhythmic variations in fragmentation[11] creating couplets of finer material

(continued on next page)

Table 2 (*continued*)

Volcanic stratigraphic units	Facies	Description	Interpretation
		by alternating sets of coarse beds with overlying finer deposits, poorly sorted. Larger blocks are commonly welded together and exhibit the largest vesicles. Clasts become slightly redder in colour and exhibit an increase in centre vesicularity and increasingly pronounced chilled rims upwards within units. Lithic to juvenile ratio ranges 100% juvenile to 37:63. Thickness not uniform, ranges 0.3–2.5 m.	through a debris filled vent[1,2] (Fig. 5a).
	SSL	Dark grey scoriaceous lapilli and spatter deposits of very fine to coarse lapilli size with blocks and some bombs up to 40 cm, that become slightly redder and exhibit an increase in centre vesicularity and increasingly pronounced chilled rims upwards, disorganised, with some alternating fine and coarse cross beds. The unit hosts non-continuous vesicular agglutinated layers that lack chilled rims and show evidence of lateral movement post-deposition. 100% juvenile. Thickness not uniform, ranges 2.2–2.9 m.	Strombolian style explosive eruptions with increased volatile content, some variation in fragmentation. Some agglutinated spatter formed by low, short-lived fountains[5] forming discontinuous clastogenic, lava flows (Fig. 5a).
Basal Unit (BU)	LT1	Pale brown lapilli tuff deposits predominantly of coarse ash to fine lapilli, with subrounded to subangular coarse lapilli lithics up to 5.5 cm, and subangular medium lapilli juvenile clasts, massive to poorly sorted, no bedding. Lithic to Juvenile ratio 75:25. Thickness 1.2 m.	Concentrated PDC formed by the collapse of an eruption column produced by a sustained period of eruption[8,10] (Fig. 4b).
	LT2	Pale grey and pale to medium brown lapilli tuff, thinly bedded with a concentrated base layer of coarse ash to fine lapilli grading normally upwards to massive coarse to fine ash. Juvenile content decreases upwards throughout the deposits. Infrequent lithic blocks of subangular orange sandstone up to 12 cm and subrounded pale grey siltstone up to 5 cm. Beds exhibit occasional undulating thickness. Lithic to juvenile ratio 43:57. Thickness ranges 0.15–0.4 m.	Pyroclastic fall deposits draped over existing deposits with common ballistic impacts from a debris filled vent[1,2] (Figs. 4b, d).
	LT3	Pale grey and pale to medium brown lapilli tuff predominantly of coarse ash to medium lapilli with subrounded lithics up to 5 cm, alternating between coarse and fine beds, inversely graded. These deposits form packages up to 26 cm thick, commonly intercalated with beds of fine to coarse ash up to 4 cm thick, draped over the coarser deposits. Packages have wavy surfaces with varying thickness. 37 cm subrounded juvenile bomb. Lithic to juvenile ratio 70:30. Thickness ranges 0.15–0.4 m.	Concentrated PDC formed by the collapse of an eruption column[8,10] with recycling of clasts[9]. Each is commonly coupled with the settling of suspended fines[1,2]. Ballistic impact of large juvenile bomb into existing unconsolidated deposits (Fig. 4d).
	TB1	Medium brown to medium grey tuff breccia predominantly of coarse ash to coarse lapilli, with subrounded to angular lithics up to 5 cm and angular juvenile clasts up to 15 cm, disorganised, no bedding, with wavy surfaces due to undulating underlying surfaces, units exhibit varying thicknesses. Lithic to juvenile ratio ranges 32:68 to 71:29. Thickness ranges 0.4–0.8 m.	Ballistic curtain deposits formed by individual explosions through a debris filled vent with some recycling of clasts[1,2,9] (Figs. 4b, d).
	TB2	Pale brown and pale grey tuff breccia, thinly bedded with a laminated base, predominantly of coarse ash to fine lapilli, occasionally alternating with medium to coarse lapilli. Subangular lithic blocks of pale grey siltstone occur up to 18 cm, as well as coarse lapilli orange sandstone lithics and angular juvenile bombs up to 5 cm, within gravity settled concentrations. Commonly grades upwards to pale brown massive coarse ash to fine lapilli. Lithic to juvenile ratio 60:40. Thickness 1.3 m.	Dilute PDC that formed along the base of a relatively stable and sustained column over a debris filled vent that provided supply of larger clasts to the traveling dilute PDCs[8,11]. The pulsating but overall sustained nature of the eruptive event is recorded by the presence of suspended fines draping coarser and lithic-rich beds[1, 2,11] (Figs. 4b, c, d).
	TB3	Pale brown and pale to medium grey tuff breccia of predominantly coarse ash with fine lapilli, with fine to medium lapilli beds, with common repeating stacks of coarse and fine deposits, cross bedded,	Concentrated PDC formed by base surges[8,10]. Flow laminated base formed by surge prior to bulk of deposit. Each PDC is commonly coupled with the settling of suspended fines[1,2]. Some recycling of clasts[9]. Lithic blocks were

(*continued on next page*)

Table 2 (*continued*)

Volcanic stratigraphic units	Facies	Description	Interpretation
		volumetrically the most dominant facies in BU. Occasional coarse ash flow laminated base, and/or thin layer of coarse ash from settling deposits on top. Beds are normally graded internally. Coarser layers of fine to medium lapilli show build up around and over lithic blocks. Lithic blocks of subrounded to subangular orange sandstone (average 25%, 11–23 cm) and subrounded pale grey siltstone (24–28 cm). Lithic to juvenile ratio ranges 35:65 to 55:45. Thickness ranges 0.8–3.8 m.	supported by the buoyancy of the surrounding flow (Figs. 4b, d).

[1](Graettinger and Valentine, 2017), [2](Graettinger et al., 2015), [3](Head and Wilson, 1989), [4](Lorenz, 1986), [5](Valentine and Gregg, 2008), [6](Parfitt and Wilson, 1995), [7](Kereszturi et al., 2014), [8](Sulpizio et al., 2014), [9](Houghton and Smith, 1993), [10](Sohn and Chough, 1989), [11](Chough and Sohn, 1990).

5.1. Volcanic stratigraphy at Wiri Mountain

Due to the differing nature of deposits, locality 1 has been split into northern and southern halves (1 N and 1S, respectively; Fig. 4a). Locality 1 N exhibits a 12.6 m tall exposure of BU deposits (Fig. 4b), as well as an angular unconformity on its southern 'edge', with slumped BU deposits and a further 0.3 m of BU deposits overlain by 1.3 m of MU deposited on top of these (Fig. 4c). Locality 1S displays 2.2 m of BU deposits exposed (Fig. 4d), followed by 0.8 m of MU deposits. The entirety of locality 1 has been overlain by CU deposits of varying thickness, up to 16.5 m thick at the centre (Fig. 5c). The stratigraphy of BU, MU and CU deposits at locality 1 is presented in Fig. 6 and Fig. 7, including juvenile to lithic ratio and lithic type based on componentry data.

Locality 2 exhibits a 14.5 m tall exposure, with 9.8 m of MU deposits overlain by 4.7 m of CU deposits (Fig. 5a). As the thickness of deposits at locality 2 vary laterally across the outcrop, these are average thicknesses and have been used in the stratigraphic column presented in Fig. 6, which summarises both juvenile to lithic ratio and lithic type based on componentry data.

Locality 3 exhibits a 1.4 m outcrop on the outer northern edge of Wiri quarry, of distal CU deposits with a rubbly top (Fig. 5b) and vesicles concentrated in bands underneath, oriented towards the north east.

Lithic clasts in outcrop at Wiri Mountain fall into two main groups: 1) very well sorted pale brown and pale grey siltstone, and 2) very well sorted medium to dark orange and orange-brown sandstone and occasional pale grey to pale brown bioclastic conglomerate sandstone. Based on known underlying stratigraphy in the area (Waterhouse, 1966; Ballance, 1976; Rout et al., 1993; Viljevac et al., 2002; Edbrooke et al., 2003; NZGD, 2016) these have been interpreted (using clast population, rock type, grain size and fossil abundance) to belong to the East Coast Bays Formation of the Waitemata Group (ECBF) and the Kaawa Formation of the Kaihu Group (KWF), respectively (Figs. 6 and 7). The total local thickness of alluvium deposited at the time of the eruption ranges between 2 and 14 m based on geotechnical boreholes (NZGD, 2016). The total thickness of the KWF varies and is dependent on paleotopography (Edbrooke et al., 2003). However based on boreholes in the immediate area, the local thickness ranges from 16 to 60 m (Viljevac et al., 2002; NZGD, 2016), with an assumed average local depth of 30 m. The KWF conformably overlies the ECBF (Viljevac et al., 2002; Edbrooke et al., 2003). The total thickness of the ECBF is unknown (Rout et al., 1993) as there are no known outcrops that show both the base and top of the formation, however it occurs up to 533 m thick at Orewa on the northern edge of the AVF (Waterhouse, 1966; Ballance, 1976) and is intercepted at an average depth of 30 m locally.

6. Grain size distribution and vesicularity

The grain size distribution of deposits at localities 1 N and 1S have a bimodal distribution, and those of locality 2 have a unimodal distribution (Fig. 8a). These deposits fall into one of two categories: 1) fine skewed grain size distribution characteristic of poorly sorted pyroclastic density current deposits, and 2) coarse skewed grain size distribution characteristic of well sorted fall beds. The deposits of locality 1 N mostly fall into category 1, with the very last (uppermost) deposits in that locality falling into category 2. Deposits of locality 1S fall into both categories and likely represent a transition between the two, and the eruptive activity the categories represent, with a general trend of category 1 in early deposits and category 2 in later (upper) deposits. Deposits of locality 2 fall into category 2.

Vesicularity results of all samples from both −4 to −5 ϕ and − 5 ϕ and above size fractions (Fig. 8b), calculated using a local DRE of 2.92 g/cm^3, are shown in Fig. 8b. The highest vesicularities recorded were taken from scoria samples at locality 2 (samples W1 and W2). The largest variation in vesicularity within a single sample occurred in juvenile lapilli at locality 1 N (sample W10).

7. Discussion

7.1. Deposit classification

The deposits of Wiri Mountain can be classified according to the volcanic stratigraphy. The BU deposits are dominantly fine-grained, rich in ash and fine lapilli-sized material (localities 1 N, 1S). The overall fine grain size of the deposits indicates their formation was through highly explosive fragmentation. The abundance of lithic material within BU and early MU deposits (Figs. 6 and 7) indicates the occurrence of subsurface eruptions that excavated pre-existing country rock. Fine-grained, cross-bedded material (in the dominant facies volumetrically in the BU deposits, Fig. 7) shows evidence of lateral transport (Facies TB3, Table 2), indicating deposition from base surge pyroclastic density current (PDC) deposition (over four times the amount by volume as fall deposits) typical of highly explosive eruptions. The wide variations in vesicularity observed in the BU deposits (e.g., sample W10, Fig. 8b) reflect the strong influence of both internal and external forces, such as internal volatile characteristics and interaction with external water. These observations indicate that BU deposits are of phreatomagmatic origin, with clasts also fragmented periodically by gas bubble outburst from a volatile-rich magma. The MU deposits are rich in juvenile material (Figs. 6 and 7), with the majority being scoria, spatter and discontinuous clastogenic lava flows, signifying increasingly degassed magma and increasing flux with limited dispersal and very little to no magma-water interaction (Parfitt, 2004; Valentine and Gregg, 2008; Sigurdsson, 2015) (Fig. 5). The CU deposits comprise entirely juvenile material and form agglutinated spatter and clastogenic deposits with little ash, typical of Hawaiian-style lava fountaining eruptions, as well as later lava flows signifying further degassing of magma (Parfitt, 2004; Valentine and Gregg, 2008; Sigurdsson, 2015).

7.2. Landform classification

The deposit architecture of the broad crater surrounded by a ring of tephra, the abundance of chilled juvenile pyroclasts and country-rock fragments (Fig. 4a), the wide range of grain sizes (Fig. 8), lithic-rich

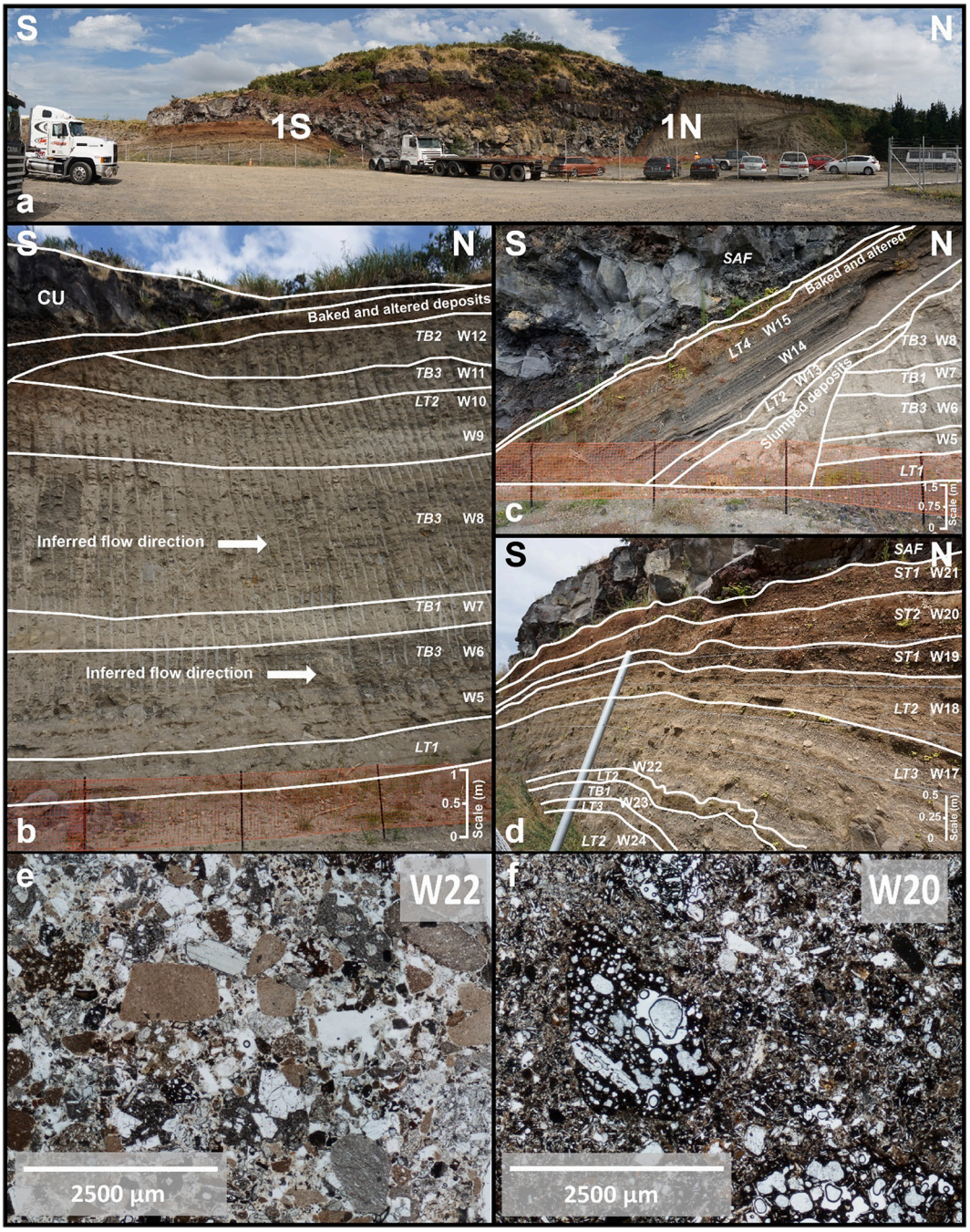

Fig. 4. Deposits exposed at Wiri Mountain: (a) Locality 1 looking west, (b) Locality 1 N located on the northern half of the exposure with inferred flow direction (based on deposit overflow and thinning of beds) shown of BU deposits (outcrop is 12.6 m high), (c) Southern side of locality 1 N, with slumped deposits and overlying Basal Unit (BU) and Middle Unit (MU) deposits, (d) Locality 1S located on the southern half of the exposure with BU, MU and Capping Units (CU) exposed towards the southern end of the outcrop (outcrop is 4.1 m high), e) Sample W22 in thin section representing typical BU deposits, and f) sample W20 in thin section, showing increase in juvenile content during transition from BU to MU deposits. Facies are labelled with prefixes T, L and S (Table 2), samples are labelled with prefix W (Figs. 6 and 7).

componentry (Figs. 6 and 7), lack of evidence of a deep 'hole in the ground' structure (Kereszturi and Németh, 2012) or lake and inward dipping bedded nature of the pyroclastic deposits at locality 1 suggest that this outcrop has cut through tuff ring deposits (Sigurdsson, 2015). Deposits from 1 N, which will be referred to as tuff ring 1 (TR1), while limited to the single tuff outcrop, show transport deposition from south to north, and host beds that dip gently towards the south (Fig. 4b). Based on historical photography, TR1 likely covered an area of approximately 0.67 km^2 (Kereszturi et al., 2014) (Figs. 3a, c). Part of the tuff ring flank was removed by an explosive blast and consequently slumped as observed on the southern 'edge' of locality 1 N (Fig. 4c). Tuff deposits from 1S, which will be referred to as tuff ring 2 (TR2), form the intact inner edge of a tuff ring with beds dipping to the north (Fig. 4d). Material that has been deposited on the steeply slumped southern 'edge' of 1 N (TR1) is interpreted to also be part of TR2 due to corresponding facies classifications (with differences between facies interpreted to be solely due to variation in underlying deposit angle, see Table 2), matching juvenile-rich nature (Fig. 6), and proximity to deposits of locality 1S. This connection between TR2 deposits and their overlying and cross-cutting relationship to that of TR1 highlights that TR1 was

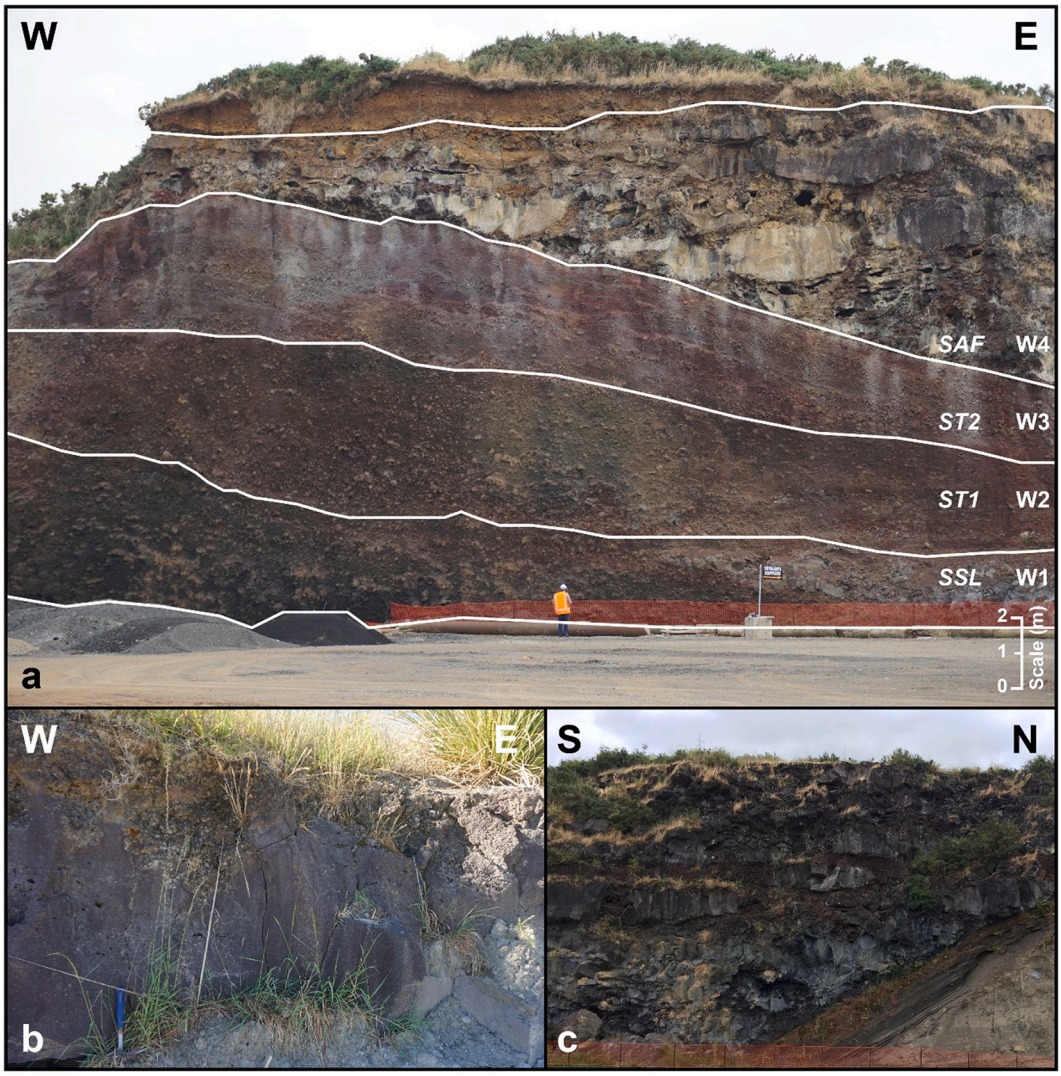

Fig. 5. Middle Unit (MU) and Capping Unit (CU) deposits at Wiri Mountain: (a) Locality 2, MU deposits and overlying CU (outcrop is 15 m high), (b) Locality 3, a cutting through distal CU deposits on the outer northern edge of the quarry (hammer for scale, outcrop is 1.4 m high), and (c) CU deposits midway along locality 1 (outcrop is 12.6 m high). Facies are labelled with prefixes T, L and S (Table 2), samples are labelled with the prefix W (Fig. 6).

deposited before TR2. The exposed deposits from TR1 and TR2 do not host correlating beds (based on visual observations, facies analysis, and componentry studies), further suggesting that they have been emplaced by different eruptions, likely from the same bladed dyke or fissure source (e.g. Pedrazzi et al., 2016) and therefore, form separate tuff rings. Based on historical photography, deposit architecture and location, TR2 is interpreted to be a small tuff ring, with a vent location to the south west of the main vent (TR1). This tuff ring was previously unreported as it was not easily visible in historical photography due to being covered by later clastogenic lava and lava flows. A second small tuff ring, which will be referred to as tuff ring 3 (TR3), was previously reported based on aerial photography (Hayward, 2015) (Fig. 3c).

The deposit architecture, componentry and their facies classifications from locality 2, as well as historical reports on the original landforms (Searle, 1959; Rout et al., 1993; Kereszturi and Németh, 2016) (Fig. 3), support the presence of an at least 90 m high coarse scoriaceous lapilli-dominated scoria cone that occupied the intra-crater region of the TR1 and eventually buried its western side.

7.3. Fragmentation depth

The ECBF is the dominant lithic type in deposits of TR1, with a minor fluctuating presence of the KWF (Fig. 7). Deposits of TR2 are also dominated by lithics of the ECBF, with KWF lithics much more abundant, up to 50% in some deposits, within the base of the tuff ring deposits (Fig. 6). However, as the host rock units of accidental lithics present in eruptive deposits can only represent the general range of depth in which explosions occurred due to active mixing and reworking in a debris-filled vent, lithic type is a poor proxy for fragmentation depth (Valentine and White, 2012; Valentine et al., 2014; Graettinger and Valentine, 2017). Scaled fragmentation depth (the relative depth of an explosion that successfully ejected material from a vent) can be inferred by applying general facies interpretations to reflect the explosion efficiency, after Graettinger and Valentine (2017) (Table 3). Near-optimal conditions, which fragment and eject the largest possible volume of material for a given energy, result in concentrated PDCs commonly coupled with associated settling of suspended fines. Shallower-than-optimal conditions are interpreted as resulting in ballistic curtains depositing massive tuff breccias, and deeper-than-optimal conditions result in most material being unable to escape the crater, with dilute PDCs depositing fine-grained material in cross-beds. It is common for the majority of deposits in a tuff ring or maar to be represented by near-optimal conditions (Graettinger and Valentine, 2017) due to the efficiency of deposition at these conditions.

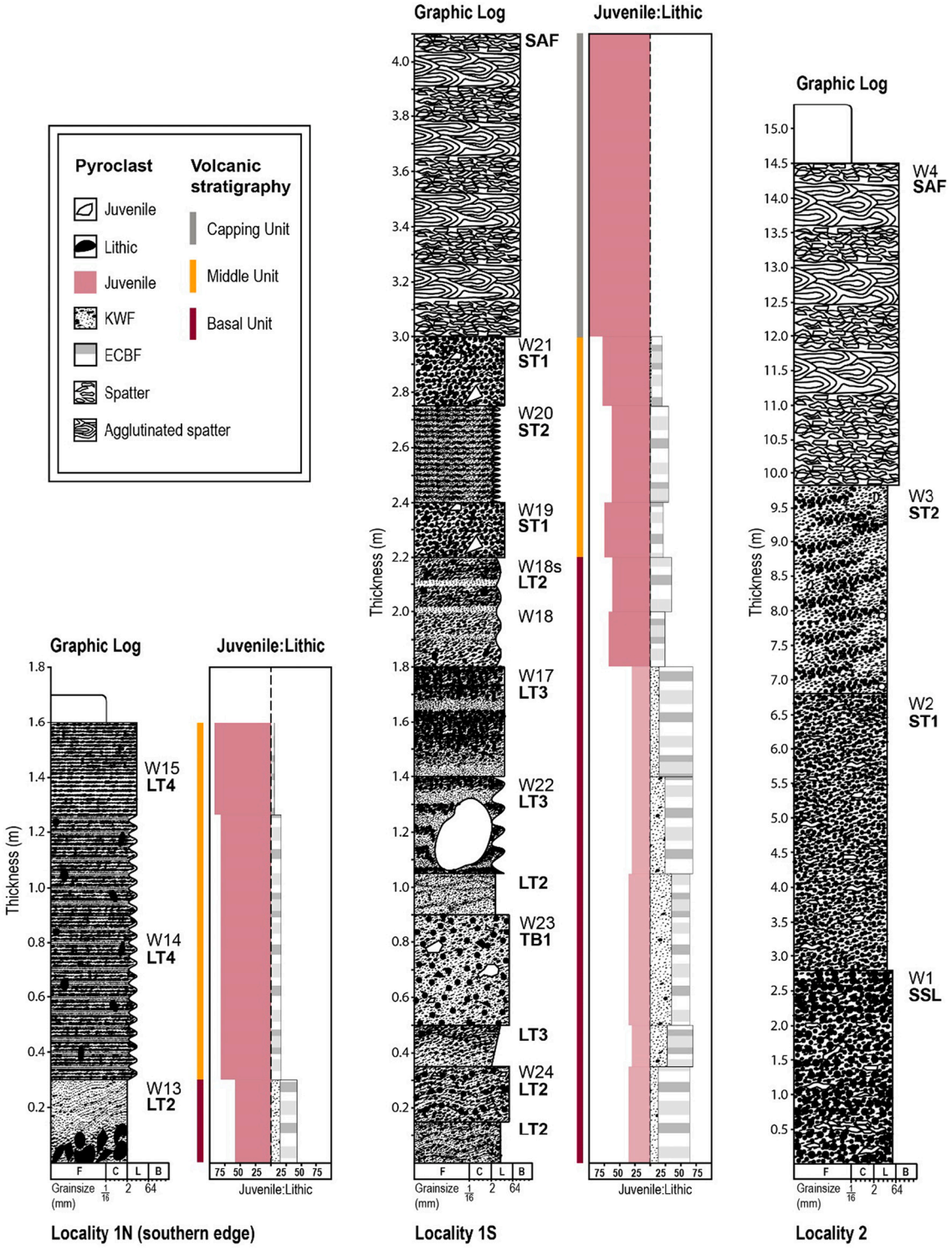

Fig. 6. Stratigraphy, juvenile to lithic ratio and lithic type componentry of Basal Unit (BU), Middle Unit (MU) and Capping Unit (CU) deposits at localities 1 N, 1S and 2 (facies in bold- see Table 2, sample numbers labelled with prefix W). Lithic types are Kaawa Formation (KWF) and East Coast Bays Formation (ECBF), see key. Grain size is shown underneath the graphic logs after Schmid (1981), with F representing fine ash, C for coarse ash, L for lapilli and B for blocks and bombs. Of all deposits over medium lapilli size, accidental lithics are shown with black fill and juvenile clasts are shown with white fill. Lithic to juvenile ratios are based on sieved componentry where possible and are represented by lighter colours where field observations were used. Lithic type is displayed as the average percentage of total lithic content across all weighed size ranges for each sample.

The interpreted scaled depths based on facies interpretations from deposits at Wiri Mountain are summarised in Table 3. In terms of accessible volume of deposits represented by each facies and scaled depth interpretation, most materials were either fragmented and ejected at near-optimal scaled depth or the transition between near-optimal and shallower/deeper depths. Very little material was fragmented and ejected at deeper than optimal scaled depth, as was expected by the model presented by Graettinger and Valentine (2017).

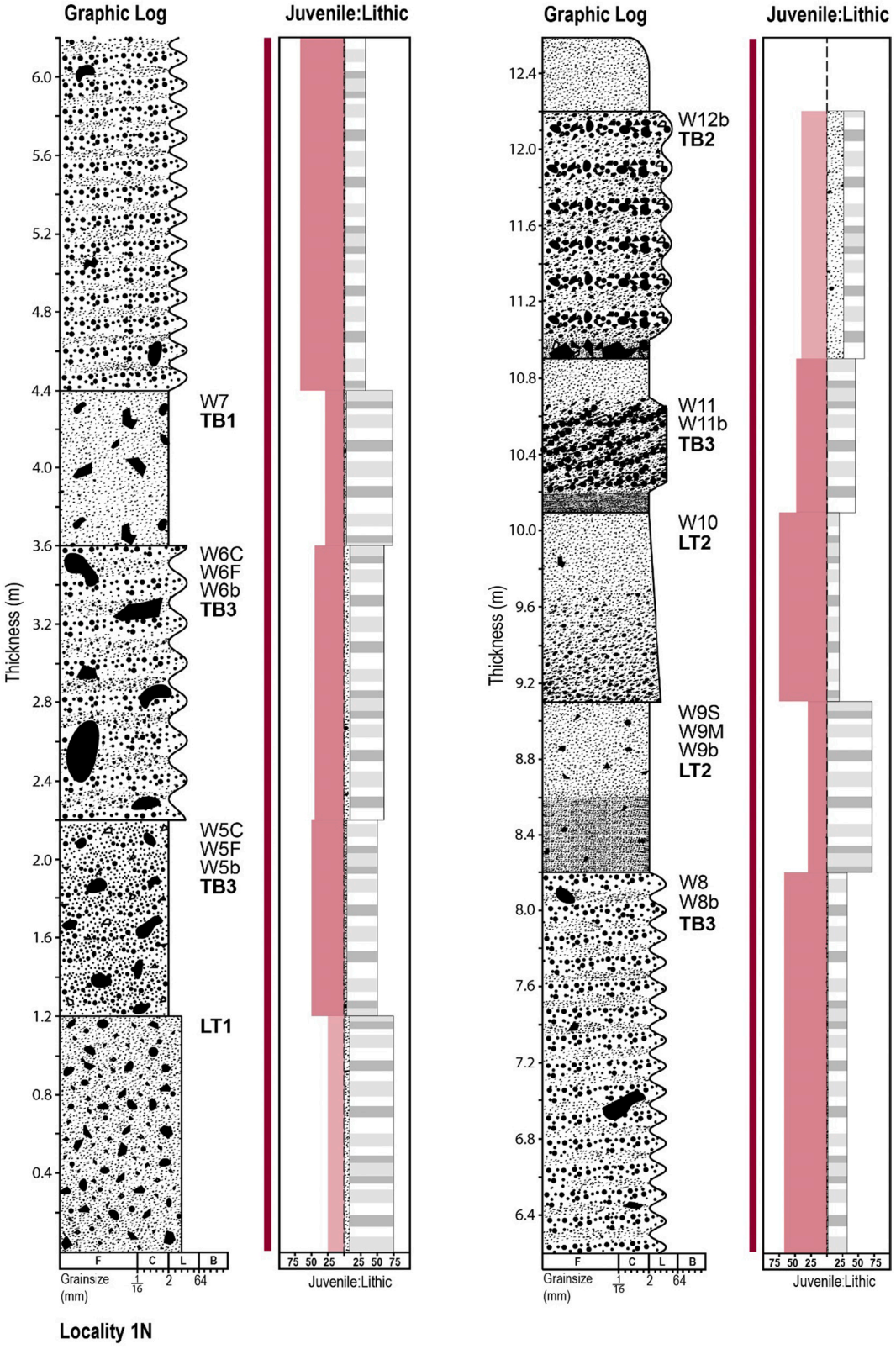

Fig. 7. Stratigraphy, juvenile to lithic ratio and lithic type componentry of Basal Unit (BU) deposits at locality 1 N (facies in bold, sample numbers labelled with prefix W). Refer to Fig. 6 for key.

7.4. Eruption history

Prior to the deposition of Wiri Mountain, the area had an irregular surface, as shown by early tuff deposits (Facies LT1), suggesting a pre-existing tuff ring/maar altered landscape likely related to one of the nearby predating volcanic centres (such as McLaughlins Hill, 48.2 ± 6.4 ka, or potentially Ash Hill, 30.7 ka ± 159 cal yr BP) (Figs. 2 and 3). This pre-existing landscape was likely subsequently eroded and covered by

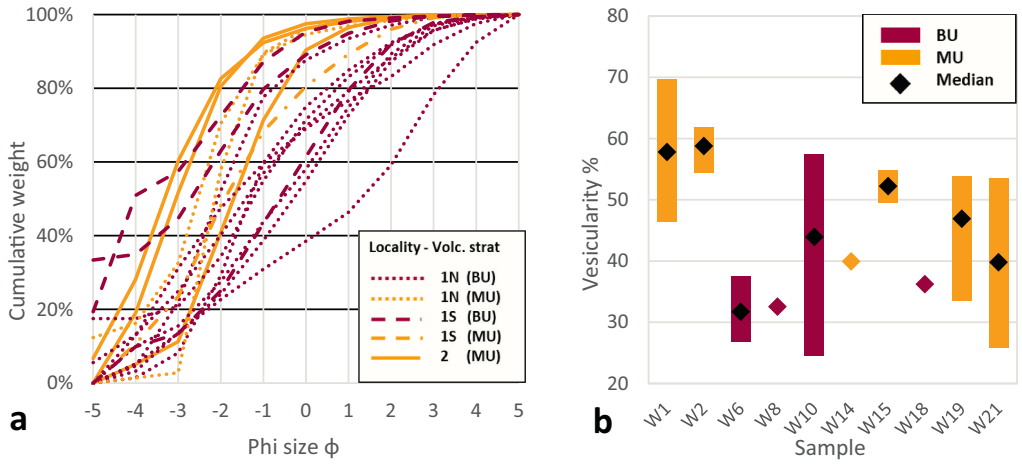

Fig. 8. a) Cumulative grain size distribution for phi sizes between −5 and 4 ϕ (category 1 in red, category 2 in orange) with corresponding volcanic stratigraphic units in key, and b) Vesicularity of juvenile samples from both −4 to −5 ϕ and − 5 ϕ and above size fractions. (For interpretation of the references to colour in this figure legend, the reader is referred to the web version of this article.)

Table 3
Scaled depth representations based on facies interpretations after Graettinger and Valentine (2017), with volcanic stratigraphic units corresponding to each facies in bold.

Facies	Scaled depth interpretation
TB1 (**BU**)	Shallower-than-optimal scaled depth discrete explosions
ST2 (**MU**)	Transition between near-optimal and shallower-than-optimal scaled depth explosions
LT3 (**BU**), TB2 (**BU**), TB3 (**BU**), ST1 (**MU**)	Abundant near-optimal scaled depth discrete explosions
LT2 (**BU**), LT4 (**MU**)	Transition between deeper-than-optimal and near-optimal scaled depth explosions
LT1 (**BU**)	Deeper-than-optimal scaled depth explosions

the accessible deposits of this study due to the abundance of water and the low-lying nature of the area. Due to the single outcrop exposure of the tuff rings, it is difficult to establish either the exact original size or location of the vent and deposits, however, estimations can be made based on dip of beds, transport direction (Fig. 4b) and historical (photographic and reported) extent of deposits (Fig. 9).

7.4.1. Tuff Ring 1

Based on historical photography and further supported by directional flow indicators observed within the deposits and the dip of beds, the vent location for the earliest exposed deposits (TR1) at Wiri Mountain was likely located to the south east of the midpoint of the main tuff outcrop. The approximate size of TR1 can be estimated from the dip of tuff beds and the lateral and vertical extent of exposed deposits (Fig. 9).

The earliest phreatomagmatic deposits of the initial basal tuff ring (Facies LT1, Fig. 4b) were deposited by the collapse of an eruption column and reflect a transforming vent phase that involved active clearing of the vent, reworking of larger proximal lithic blocks and deep excavation of the juvenile lining of the pre-eruption vent or older cooled juvenile material (Fig. 10a). A sustained period of deposition then occurred with numerous high particle concentration PDCs (Facies TB3, Figs. 4b, 7) formed by base surges coupled with the eventual settling of associated suspended fines, and excavation of juvenile material (e.g., lining of the vent) at near-optimal depth (Table 3, Fig. 10b). Excavation of country-rock in the ECBF continued to change vent morphology by widening deeper in the conduit (Fig. 7). Shallow individual explosions through the debris-filled vent (Facies TB1, Fig. 4b) formed ballistic curtain deposits rich in accidental ECBF lithics. A prolonged period of deposition then occurred once again with numerous high particle concentration PDCs (Facies TB3, Figs. 4b, 7) formed by base surges coupled with the eventual settling of suspended fines, and continued excavation of the juvenile lining of the vent at near-optimal depth (Table 3). A short period of increased moderately deep (ECBF in this area ranges from 30 m to >200 m) fragmentation from a debris-filled vent (Facies LT2) formed an eruption column that produced pyroclastic fall beds with common ballistic impacts (Fig. 10c). Ejection of lithic material from the vent decreased as fragmentation was drawn deeper (Fig. 7). Base surges then produced high particle concentration PDCs (Facies TB3), shallow excavation and reworking of the juvenile vent lining and country-rock of the ECBF, depositing lithic-rich cross-beds and eventually settled finer material (Figs. 7, 10d). The vent then entered a phase of highly efficient vent clearing at near-optimal depth (Table 3), considerably changing the conduit and inner crater morphology (coarse deposits rich in angular lithics of both ECBF and KWF). The eruption column continued to be relatively stable and sustained, with a debris filled vent that provided larger clasts to the dilute PDCs forming over the base of the column (Facies TB2, Fig. 4b). Rhythmic variations in fragmentation caused pulses in the sustained column and deposited packets of alternating coarse and fine lithic-rich beds draped with suspended fines (Fig. 7).

The phreatomagmatic eruptive activity producing deposits in this location suggests a steady source of water to fuel magma-water interactions was present throughout the time that the eruption produced BU deposits (e.g., Valentine et al., 2014). Groundwater hosted mainly by the KWF and to a lesser extent the ECBF is the most likely source of these interactions due to the high permeability of the unit (Viljevac et al., 2002), the lithic content of the tuff deposits (dominantly KWF, Figs. 6 and 7), and the facies implications on explosive depths (limited fragmentation and ejection of deeper-than-optimal scaled depths, Table 3).

7.4.2. Tuff Ring 2

A second smaller vent then punctured through the existing tuff ring flank to the south-west of the main vent (Fig. 9, 10e), in an initial clearing explosive event before further significant deposition began. The location of the second vent and the approximate tuff ring size is based on the intact inner edge of the tuff ring as seen in the outcrop and the dip of beds on the northern edge of its exposure (Fig. 9).

Basal phreatomagmatic deposits of the tuff ring were deposited on an irregular surface (Fig. 4d), caused by the explosive initial clearing of the vent and likely subsequent slumping and collapse of the surrounding tuff ring deposits. Early stages of the phreatomagmatic eruption produced pyroclastic fall deposits with common ballistic impacts, rich in accidental lithics (Facies LT2, Fig. 6), with moderately deep fragmentation

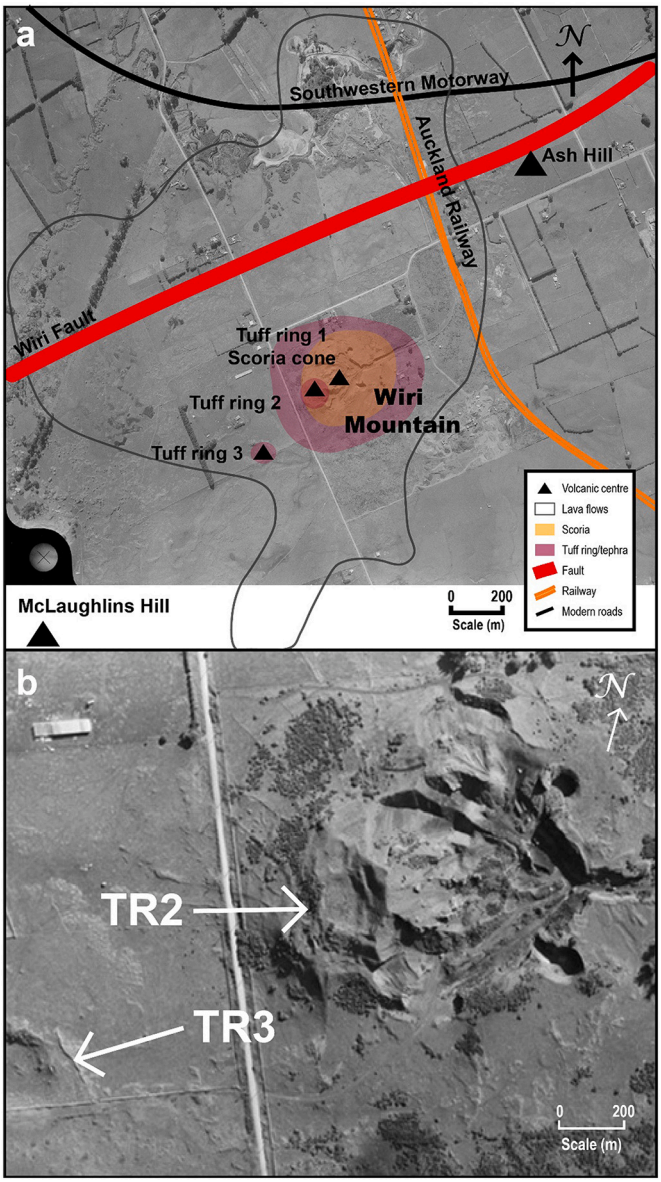

Fig. 9. a) Vent locations and deposits of Wiri Mountain, with the approximate location of the Wiri Fault (Kenny et al., 2012), main roads and railway for reference. Satellite photo from LGGA (1925). Wiri Mountain lava flow deposit boundary line inferred from Kermode (1992); Edbrooke (2001); and Edbrooke et al. (2003), b) Aerial photography showing the location of the TR2 and TR3 craters (Whites Aviation, 1958).

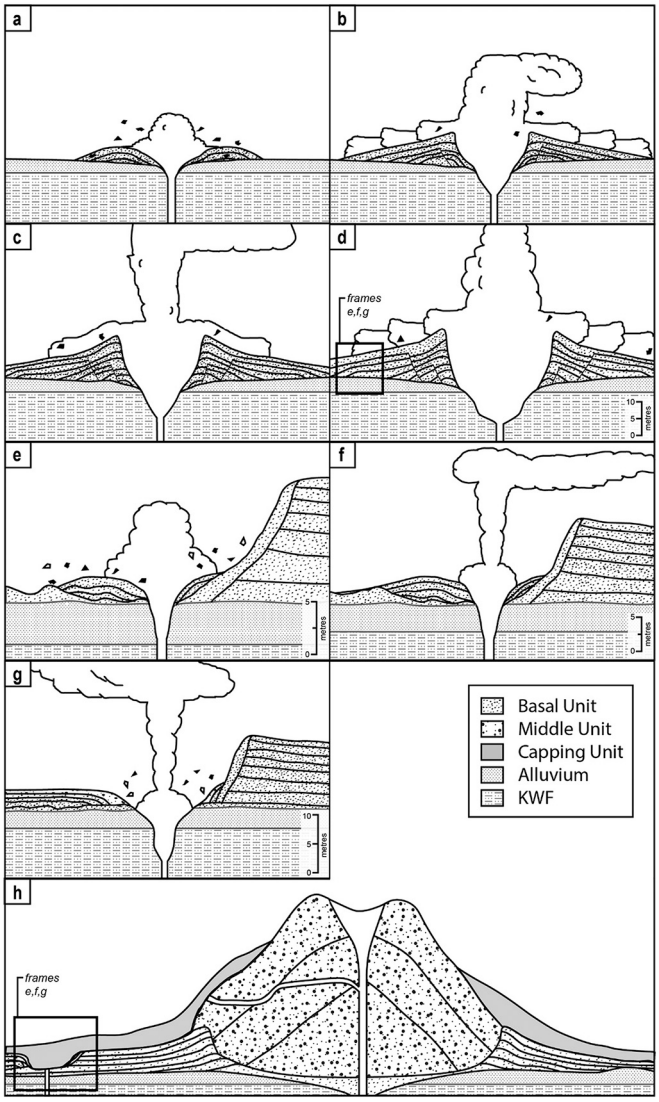

Fig. 10. Simplified cartoon diagram (looking north) of some of the representative stages of the eruption history of Wiri Mountain: a) TR1 transforming vent phase, widening and active clearing of vent, lithic-rich surge deposits; b) Fragmentation is drawn deeper, PDCs and ballistic curtain deposits rich in accidental lithics; c) Deep fragmentation, pyroclastic fall with common ballistic impacts; d) Sustained period of fragmentation, shallow excavation and reworking at depth, fall and surge deposits; e) TR2 erupted through flanks of TR1, deep fragmentation, pyroclastic fall with ballistic impacts followed by PDCs; f) Fragmentation at moderate depth, conduit widening both shallow and deep, pyroclastic fall with ballistic impacts; g) Transition phase from phreatomagmatic to magmatic activity, increasing juvenile content, Strombolian fall deposits; h) Scoria cone (TR1 vent) deposited, transition to explosive magmatic Strombolian activity, scoria and spatter deposits, filled TR1 and buried the western side, eventual transition to effusive activity, clastogenic lava flows and lava flows cover the area. KWF shown in key is the Kaawa Formation.

(Table 3) through a debris-filled vent. Collapses of the eruption column then produced high particle concentration PDCs coupled with the eventual settling of suspended fines (Facies LT3, Fig. 4d), near-optimal excavation of the juvenile lining of the vent (Table 3) and reworking of accidental lithics within the vent. Vent morphology continued to reflect widening and country-rock excavation at the (near) surface and at depth (Fig. 10e). Individual shallow explosions formed ballistic curtain deposits rich in accidental lithics (Facies TB1), followed by potentially settling-related (Graettinger and Valentine, 2017) pyroclastic fall deposits from eruption columns with common ballistic impacts of accidental lithic-rich material (Facies LT2, Fig. 4e) erupted at moderate depth (Table 3) through a debris-filled vent (Fig. 10f). The eruption column again collapsed, forming high particle concentration pyroclastic density currents coupled with the eventual settling of associated suspended fines (Facies LT3, Fig. 4d), and continued excavation of the juvenile lining of the vent at near-optimal depth (Table 3). The vent continued to widen both at the (near) surface and at depth (Fig. 10f).

An angular unconformity formed on part of the inner southern edge of the initial basal tuff ring (Fig. 4c), either by gravity-led slumping of tuff deposits into the crater, or by erosion from the early eruptive activity of the smaller tuff ring (Graettinger et al., 2015). The slumped deposits provided a sufficient surface to allow deposition onto pre-existing deposits of the first tuff ring that were originally too steep for permanent deposition to occur.

The eruption then entered a gradual transition phase. Later deposits of TR2 represent the transition from 'wet' phreatomagmatic eruptions to

more 'dry' magmatic Strombolian eruptions over time (Figs. 4c, d, 6), a common trend of the eruption progressions in both the AVF and other monogenetic fields (e.g., Allen et al., 1996; Houghton et al., 1999; Kereszturi et al., 2014), suggesting a dwindling supply rate or access to an external source of water to fuel magma water interactions (through sealing of the conduit or depletion of local groundwater resources), or an increase in magma flux, or both (Lorenz, 1986; Head and Wilson, 1989; Valentine and White, 2012; Kereszturi et al., 2014; Németh and Kósik, 2020).

The succeeding deposits were juvenile-rich fall (Facies LT2, ST1, Fig. 4d) and curtain deposits with increasing vesicularity (Fig. 8b) followed by packages of coarse and fine material (Facies ST2, Fig. 4f). These represent periods of Strombolian eruptions with moderately deep fragmentation, followed by rhythmic variations in moderate to shallow fragmentation (Table 3) with minor recycling of material through a debris-filled vent as minor pyroclastic influence decreased over time (Fig. 10g). The corresponding deposits on the slumped edge of the basal tuff ring vary in appearance due to differences in deposit angle and proximity to the vent and exhibit stronger bedding overall (Facies LT2, LT4, Fig. 4c).

7.4.3. Scoria Cone

After the formation of the main tuff ring and the second smaller tuff ring, volcanic activity continued at the location of the main vent to produce a large central scoria cone within TR1 (Figs. 3a, 5a, 6, 9). Based on an assumed average flank slope of 30° (Kereszturi and Németh, 2012) and an estimated original height of 90 m (Searle, 1961; Rout et al., 1993), the estimated surface area of the scoria cone is shown in Fig. 9. The transition from phreatomagmatic to a more magmatic-dominated eruption style and scoria cone growth represents a further increase in magma flux and a large enough volume of melt available (e.g., Head and Wilson, 1989; Valentine and White, 2012; Németh and Kósik, 2020), eventually leading to a rapid transition to magmatic activity in the later stages of the eruption. Strombolian-style eruptive activity deposited scoria and spatter that occasionally welded together in places and commenced minor lateral clastogenic lava flows (Facies SSL, Figs. 5a, 6), indicating periodic increases in accumulation rate (Parfitt and Wilson, 1995; Parfitt, 2004) (Fig. 10h). Strombolian-style eruptions continued with rhythmic variations in fragmentation, creating packages with finer material (Facies ST1, ST2, Figs. 5a, 6). The scoria cone eventually filled most of the initial basal tuff ring (TR1), obscuring and partially burying the phreatomagmatic deposits on their western side (Figs. 3a, 10h).

7.4.4. Lava spatter and lava flows

There is no evidence of significant vent movement after this point, suggesting the same vent later hosted a final transition from Strombolian to Hawaiian style eruptions and intensive effusive eruptive activity (e.g., Parfitt and Wilson, 1995). This indicates a combination of the diminishing of external water sources to sustain phreatomagmatic activity and a likely increase in magma flux and potential lining of conduit walls by chilled magma, evidenced by the large volume of lava production in the final stage of the eruption (e.g., Head and Wilson, 1989). The scoria cone deposits were partially covered (Searle, 1961; Rout et al., 1993) (Fig. 5a), along with all the underlying tuff rings (Firth, 1930) (Fig. 5c), by alternating agglutinated lava spatter forming some clastogenic flows and rubbly pahoehoe to a'a lava flows (Facies SAF, Fig. 6), which eventually became the dominant deposit produced, flowing over the tuff ring and beyond to the north and west (Figs. 5b, 9a, 10h). Where the lava and spatter covered the tuff rings, the tuff was baked and subsequently formed an altered rim (Fig. 4b). Lava breached the scoria cone in multiple locations to supply these lava flows, as mentioned by Searle (1961) and Rout et al. (1993) (Fig. 10h). This is evidenced by the Wiri lava cave burying underneath and through scoria cone deposits before breaching the surface near the base of the scoria cone (Hayward and Crossley, 2014) and the existence of lava flows covering the lower flanks of the scoria cone (Figs. 5a and 6). The extent of the effusive lava flows can be estimated based on historical reports, historical photography, and field observations (Kermode, 1992; Edbrooke, 2001; Edbrooke et al., 2003) (Figs. 3c, 9).

7.4.5. Tuff Ring 3

A third, small tuff ring was created on the distal extents of the initial basal tuff ring to the southwest. The location of the tuff ring can be seen in Fig. 9 and an approximate diameter of 100 m is estimated from aerial photography taken before the landform was removed (Hayward, 2015). Due to the lack of remaining deposits, the timeline of the formation of this tuff ring is uncertain.

7.5. Volcanic field-scale implications

Magma ascent at Wiri Mountain volcanic complex and nearby centres (Mc Laughlins Hill, Puhinui Craters and Ash Hill) (Fig. 2) was likely aided by faults like the inferred subsurface Wiri Fault (Von Veh and Németh, 2009; Kenny et al., 2012; Kereszturi et al., 2014). Activity at Wiri Mountain and Ash Hill could have been part of the same episode (Hayward, 2008; Kereszturi et al., 2013), potentially along a fault-controlled fissure (e.g., Kósik et al., 2016). The two smaller craters from Wiri Mountain included in this study were also strongly aligned with the Wiri Fault (Fig. 9a). Considering the fractured nature of the host rocks, and the wide coverage of lava flows from both Wiri Mountain and McLaughlins Hill, small associated craters were probably more prevalent in the area than can be confirmed (Searle, 1961).

Volcanic activity in the AVF has generally been characterised by phreatomagmatic, Strombolian or effusive eruption styles, or a combination of these (Kereszturi and Németh, 2016). There are several examples where eruptive activity has been strongly influenced by the complex interplay between magma flux, the available groundwater and its recharge conditions (e.g., Houghton et al., 1996; McGee et al., 2012; Németh et al., 2012; Agustín-Flores et al., 2014; Brenna et al., 2018; Hayward, 2018). At Wiri Mountain, the transition from an initial phreatomagmatic to subsequent magmatic explosive and effusive phases fits well to the general understanding of the eruption style changes over time from other larger and more complex volcanoes of Auckland (e.g., Kereszturi et al., 2014). The transition recorded at Wiri Mountain from 'wet' phreatomagmatic eruptions to 'dry' Strombolian and Hawaiian eruptions is not unique to the AVF, and there are examples both elsewhere in New Zealand (e.g., Mt. Ruapehu, Kósik et al., 2016) and worldwide, such as in the East Eifel Volcanic Field in Germany (Houghton and Schminke, 1986), the Bakony-Balaton Highland Volcanic Field in Hungary (Kereszturi et al., 2010), Harrat Rahat in Saudi Arabia (Murcia et al., 2015), the Durango Volcanic Field in Mexico (Aranda-Gómez et al., 1992) and the Newer Volcanics Province in Australia (van Otterloo et al., 2013).

7.6. Hazard implications

In the context of Auckland volcanic hazard and future eruption scenarios, Wiri Mountain provides a striking example of an eruption that was fed by relatively stable melt sources, such that even in a well-drained coastal region, initial phreatomagmatic phases could be overridden by subsequent magmatic explosive and effusive phases because sustained magma flux and a large enough volume of melt was available (e.g., Kereszturi et al., 2014). The low-lying nature of the region promotes "one-shot" phreatomagmatic explosion craters to form if magma rises along a system with temporary rises outside of the more established magma rise zones. Such eruptions have been inferred to produce the TR3 and potentially other suspected explosion craters nearby Wiri Mountain. If magma output is slightly elevated, the "one-shot" phreatomagmatic explosion craters quickly turn to be more sustained phreatomagmatic volcanoes such as shallow maars and tuff rings with slightly thicker tephra rims. Wiri Mountain has also shown that a likely fault-controlled eruption along a fissure following initial phreatomagmatic phases could

evolve to a complex large volume scoria cone if an established conduit is able to develop. Wiri Mountain has a large enough eruptive volume to allow a complex eruptive evolution over time (e.g., Kereszturi et al., 2014), multiple smaller eruptions (Hayward et al., 2012; Hayward, 2015), with a potential connection to other centres (Hayward, 2008; Hopkins et al., 2017).

8. Conclusions

Despite significant destruction of the volcanic deposits of Wiri Mountain, the remaining outcrops and exposures presented an excellent opportunity to examine the early phases of the eruption and the growth of monogenetic volcanoes. Wiri Mountain had a complex eruption history and was deposited on a pre-existing tuff ring/maar landscape. An initial basal tuff ring was deposited by predominantly pyroclastic density currents with ballistic curtain deposits and some pyroclastic fall through a debris-filled vent that widened mostly at depth through the course of the eruptions. These early deposits reflect a steady source of water to fuel magma-water interactions. At least two smaller tuff rings were then deposited on the outer flanks of the first by a combination of pyroclastic density currents and pyroclastic fall, with a transition from phreatomagmatic to Strombolian eruptive style. These deposits reflect a dwindling access or supply rate to water. A central scoria cone was then built within the initial tuff ring, followed by lava spatter, clastogenic lava flows and lava flows that covered all three tuff rings, part of the scoria cone and the surrounding area. These later deposits reflect a combination of the diminishing of external water sources required to sustain phreatomagmatic activity and a likely increase in magma flux and potential lining of conduit walls by chilled magma. This complex eruption history reflects how small magma volumes typically involved in monogenetic volcanism allow for significant influence of fragmentation and eruptive products by the complex interplay between magma flux, the available groundwater and its recharge conditions. This complex eruption history also highlights both gradual and rapid transitions of eruptive activity and styles, leading to the creation of multiple types of eruptive products and deposits typical for the AVF. Based on the results of this study, volcanic activity at Wiri Mountain and the surrounding area of the southern end of the AVF was potentially more complex than would typically be expected from the textbook definition of monogenetic activity. The dramatically fine balance between the external and internal conditions that govern the growth of Auckland volcanoes is clearly showcased in such examples as Wiri Mountain, and its complexity helps to highlight the grey area on the concept boundary of monogenetic volcanism.

This study yields important insight into the growth and evolution of volcanoes in the AVF. Initial phreatomagmatic explosive activity aligned along fissures implicates multi-vent eruption hazards in a relatively short timeframe, and the example shown at Wiri Mountain could characterise the initial stage of a future eruption in the AVF.

CRediT authorship contribution statement

April Foote: Conceptualization, Methodology, Validation, Investigation, Resources, Writing – original draft, Writing – review & editing, Visualization, Project administration. **Károly Németh:** Conceptualization, Methodology, Validation, Investigation, Writing – review & editing, Supervision. **Heather Handley:** Conceptualization, Validation, Writing – review & editing, Supervision, Funding acquisition.

Declaration of Competing Interest

The authors declare that they have no known competing financial interests or personal relationships that could have appeared to influence the work reported in this paper.

Data availability

Data will be made available on request.

Acknowledgements

We thank Boglárka Németh for her assistance in the field and for providing geoheritage perspectives. We are grateful to Hick Bros Civil Construction Ltd. for access to Wiri quarry. We acknowledge Peter Wieland and Manal Bebbington at Macquarie University for laboratory assistance. AF appreciates discussions on the AVF with Jan Lindsay (DEVORA) and thanks Tracey Howe for access to the New Zealand Geotechnical Database. We thank two anonymous reviewers for constructive comments that have improved the manuscript. We thank José Luis Macías for editorial handling of this manuscript. This study was supported by a Macquarie University Research Training Program Scholarship awarded to AF and an Australian Research Council Discovery Project (DP150100328) awarded to HH.

References

Agustín-Flores, J., Németh, K., Cronin, S., Lindsay, J.M., Kereszturi, G., Brand, B.D., Smith, I.E.M., 2014. Phreatomagmatic eruptions through unconsolidated coastal plain sequences, Maungataketake, Auckland Volcanic Field (New Zealand). J. Volcanol. Geotherm. Res. 276, 46–63.

Allen, S.R., Smith, I.E.M., 1994. Eruption styles and volcanic hazard in the Auckland Volcanic Field, New Zealand. Geosci. Rep. Shizuoka University 5–14.

Allen, S.R., Bryner, V.F., Smith, I.E.M., Ballance, P.F., 1996. Facies analysis of pyroclastic deposits within basaltic tuff-rings of the Auckland volcanic field, New Zealand. N. Z. J. Geol. Geophys. 39, 309–327.

Aranda-Gómez, J.J., Luhr, J.F., Pier, G., 1992. The La Breña—El Jagüey Maar Complex, Durango, México: I Geological evolution. Bull. Volcanol. 54, 393–404.

Ballance, P.F., 1976. Stratigraphy and bibliography of the Waitemata Group of Auckland, New Zealand. N. Z. J. Geol. Geophys. 19, 897–932.

Bebbington, M.S., Cronin, S., 2011. Spatio-temporal hazard estimation in the Auckland Volcanic Field, New Zealand, with a new event-order model. Bull. Volcanol. 73, 55–72.

Berry, K.A., 1986. Stratigraphic, Structural and Geophysical Studies of Neogene Sediments of the Manukau Lowlands. Unpublished MSc thesis:. University of Auckland.

Brenna, M., Cronin, S., Kereszturi, G., Sohn, Y.K., Smith, I.E.M., Wijbrans, J., 2015a. Intraplate volcanism influenced by distal subduction tectonics at Jeju Island, Republic of Korea. Bull. Volcanol. 77, 1–16.

Brenna, M., Németh, K., Cronin, S., Sohn, Y.K., Smith, I.E.M., Wijbrans, J., 2015b. Co-located monogenetic eruptions ~200 kyr apart driven by tapping vertically separated mantle source regions, Chagwido, Jeju Island, Republic of Korea. Bull. Volcanol. 77.

Brenna, M., Cronin, S.J., Smith, I.E.M., Tollan, P.M.E., Scott, J.M., Prior, D.J., Bambery, K., Ukstins, I.A., 2018. Olivine xenocryst diffusion reveals rapid monogenetic basaltic magma ascent following complex storage at Pupuke Maar, Auckland Volcanic Field, New Zealand. Earth Planet. Sci. Lett. 499, 13–22.

Briggs, R.M., Okada, T., Itaya, T., Shibuya, H., Smith, I.E.M., 1994. K-Ar ages, paleomagnetism, and geochemistry of the South Auckland volcanic field, North Island, New Zealand. N. Z. J. Geol. Geophys. 143–153.

Cas, R.A.F., Wright, J.V., 1988. Volcanic Successions. Chapman & Hall, London, pp. 1–528.

Cassata, W.S., Singer, B.S., Cassidy, J., 2008. Laschamp and Mono Lake geomagnetic excursions recorded in New Zealand. Earth Planet. Sci. Lett. 268, 76–88.

Cassidy, J., Locke, C.A., 2010. The Auckland volcanic field, New Zealand: Geophysical evidence for structural and spatio-temporal relationships. J. Volcanol. Geotherm. Res. 195, 127–137.

Chough, S.K., Sohn, Y.K., 1990. Depositional mechanics and sequences of base surges, Songaksan tuff ring, Cheju Island, Korea. Sedimentology 37, 1115–1135.

Collections, S.G.G.S., 1922. Ballast for the railways: a volcanic hill at Wiri, south of Auckland, from whence a supply is obtained. In: Supplement to the Auckland Weekly News 30 March 1922 p041. Auckland Libraries, Auckland.

DOC, 1990. In: Conservation, D.O. (Ed.), Report of the Protection of the Wiri Lava Cave. Parliamentary Commissioner for the Environment, Wellington, New Zealand.

Edbrooke, S.W., 2001. Geology of the Auckland Area: Scale 1:250 000. Institute of Geological and Nuclear Sciences, New Zealand.

Edbrooke, S.W., Mazengarb, C., Stephenson, W., 2003. Geology and geological hazards of the Auckland urban area, New Zealand. Quat. Int. 103, 3–21.

Firth, C.W., 1930. The geology of the north-west portion of Manukau County, Auckland. New Zealand Sci. Congress 85–137.

Fisher, R.V., 1966. Rocks composed of volcanic fragments and their classification. Earth Sci. Rev. 1, 287–298.

Fisher, R.V., Schminke, H.-U., 1984. Pyroclastic Rocks. Library of Congress, Berlin, pp. 1–472.

GNS, 2020. NZL GNS 1:250K Geology, 3rd edition. GNS Science, Lower Hutt, New Zealand.

Google., 2020. *Wiri, Auckland, New Zealand* [Online]. Google. Available. https://earth.google.com/web/@-37.00938071,174.8587874,36.76691211a,4690.45300749d,35y,0h,0t,0r (Accessed 20/05/2020).
Graettinger, A.H., Valentine, G.A., 2017. Evidence for the relative depths and energies of phreatomagmatic explosions recorded in tephra rings. Bull. Volcanol. 79.
Graettinger, A.H., Valentine, G.A., Sonder, I., Ross, P.-S., White, J.D.L., 2015. Facies distribution of ejecta in analog tephra rings from experiments with single and multiple subsurface explosions. Bull. Volcanol. 77, 1–12.
Grant-Taylor, T.L., Rafter, T.A., 1971. New Zealand radiocarbon age measurements - 6. N. Z. J. Geol. Geophys. 14, 364–402.
Gravis, I., Németh, K., Twemlow, C., Németh, B., 2020. The case for community-led geoheritage and geoconservation ventures in Māngere, South Auckland, and Central Otago, New Zealand. Geoheritage 12, 1–24.
Green, R.M., Bebbington, M.S., Cronin, S.J., Jones, G., 2014. Automated statistical matching of multiple tephra records exemplified using five long maar sequences younger than 75 ka, Auckland, New Zealand. Quat. Res. 82, 405–419.
Hayes, J.L., Wilson, T.M., Deligne, N.I., Lindsay, J.M., Leonard, G.S., Tsang, S.W.R., Fitzgerald, R.H., 2020. Developing a suite of multi-hazard volcanic eruption scenarios using an interdisciplinary approach. J. Volcanol. Geotherm. Res. 392, 106763.
Hayward, B.W., 2008. Ash Hill Volcano, Wiri. Geocene. Geoscience Society NZ, pp. 8–9.
Hayward, B.W., 2015. Small satellite explosion craters in the Auckland Volcanic Field [Online]. Available: https://scholar.googleusercontent.com/scholar?q=cache:iBjBvV0zpYwJ:scholar.google.com/+hayward+2015+small+satellite+&hl=en&as_sdt=0,5&inst=9337400240212475524.
Hayward, B.W., 2018. An explanation for the origin of the triangular tuff ring remnants at Puketutu volcano. Geocene 19, 16–18.
Hayward, B.W., Crossley, P.C., 2014. Why Wiri lava cave is so special. Geosci. Soc. New Zealand Newsletter 13, 18–24.
Hayward, B.W., Murdoch, G., Maitland, G., Jamieson, A., 2011. Volcanoes of Auckland: The Essential Guide. Auckland University Press, Auckland, p. 234.
Hayward, B.W., Kenny, J.A., Grenfell, H., 2012. Puhinui Craters. Geocene. Geoscience Society of New Zealand, pp. 14–18.
Head, J.W., Wilson, L., 1989. Basaltic pyroclastic eruptions: influence of gas-release patterns and volume fluxes on fountain structure, and the formation of cinder cones, spatter cones, rootless flows, lava ponds and lava flows. J. Volcanol. Geotherm. Res. 37, 261–271.
Hopkins, J.L., Wilson, C.J.N., Milled, M., Leonard, G.S., Timm, C., McGee, L.E., Smith, I.E.M., Smith, E.G.C., 2017. Multi-criteria correlation of tephra deposits to source centres applied in the Auckland Volcanic Field, New Zealand. Bull. Volcanol. 0–35.
Hopkins, J.L., Smid, E.R., Eccles, J.D., Hayes, J.L., Hayward, B.W., McGee, L.E., van Wijk, K., Wilson, T.M., Cronin, S.J., Leonard, G.S., Lindsay, J.M., Németh, K., Smith, I.E.M., 2020. Auckland Volcanic Field magmatism, volcanism, and hazard: a review. N. Z. J. Geol. Geophys. 1–22.
Houghton, B.F., Schminke, H.-U., 1986. Mixed deposits of simultaneous strombolian and phreatomagmatic volcanism: Rothenberg volcano, East Eifel volcanic field. J. Volcanol. Geotherm. Res. 30, 117–130.
Houghton, B.F., Smith, R.T., 1993. Recycling of magmatic clasts during explosive eruptions: estimating the true juvenile content of phreatomagmatic volcanic deposits. Bull. Volcanol. 55, 414–420.
Houghton, B.F., Wilson, C.J.N., 1989. A vesicularity index for pyroclastic deposits. Bull. Volcanol. 51, 451–462.
Houghton, B.F., Wilson, C.J.N., Rosenburg, M.D., Smith, I.E.M., Parker, R.J., 1996. Mixed deposits of complex magmatic and phreatomagmatic volcanism: an example from Crater Hill, Auckland, New Zealand. Bull. Volcanol. 58, 59–66.
Houghton, B.F., Wilson, C.J.N., Smith, I.E.M., 1999. Shallow-seated controls on styles of explosive basaltic volcanism: a case study from New Zealand. J. Volcanol. Geotherm. Res. 97–120.
Kawabata, E., Bebbington, M.S., Cronin, S.J., Wang, T., 2016. Optimal likelihood-based matching of volcanic sources and deposits in the Auckland Volcanic Field. J. Volcanol. Geotherm. Res. 323, 194–208.
Kenny, J.A., Lindsay, J.M., Howe, T.M., 2012. Post-Miocene faults in Auckland: Insights from borehole and topographic analysis. N. Z. J. Geol. Geophys. 55, 323–343.
Kereszturi, G., Németh, K., 2012. Monogenetic basaltic volcanoes: genetic classification, growth, geomorphology and degradation. In: Németh, K. (Ed.), Updates in Volcanology - New Advances in Understanding Volcanic Systems. IntechOpen, London.
Kereszturi, G., Németh, K., 2016. Sedimentology, eruptive mechanism and facies architecture of basaltic scoria cones from the Auckland Volcanic Field (New Zealand). J. Volcanol. Geotherm. Res. 324, 41–56.
Kereszturi, G., Németh, K., Csillag, G., Balogh, K., Kovács, J., 2010. The role of external environmental factors in changing eruption styles of monogenetic volcanoes in a Mio/Pleistocene continental volcanic field in western Hungary. J. Volcanol. Geotherm. Res. 201, 227–240.
Kereszturi, G., Németh, K., Csillag, G., Balogh, K., Kovács, J., 2011. The role of external environmental factors in changing eruption styles of monogenetic volcanoes in a Mio/Pleistocene continental volcanic field in western Hungary. J. Volcanol. Geotherm. Res. 201, 227–240.
Kereszturi, G., Németh, K., Cronin, S.J., Agustín-Flores, J., Smith, I.E.M., Lindsay, J., 2013. A model for calculating eruptive volumes for monogenetic volcanoes-Implication for the Quaternary Auckland Volcanic Field, New Zealand. J. Volcanol. Geotherm. Res. 16–33.
Kereszturi, G., Németh, K., Cronin, S., Procter, J., Agustín-Flores, J., 2014. Influences on the variability of eruption sequences and style transitions in the Auckland Volcanic Field, New Zealand. J. Volcanol. Geotherm. Res. 286, 101–115.
Kermode, L., 1992. Geology of the Auckland Urban Area. Institute of Geological and Nuclear Science, Lower Hutt, New Zealand.
Kermode, L., 1994. New Zealand lava caves worth preserving for their geologic and geomorphic features. In: Geoscience Reports of Shizuoka University, 20, pp. 15–24.
Kósik, S., Németh, K., Kereszturi, G., Procter, J.N., Zellmer, G.F., Geshi, N., 2016. Phreatomagmatic and water-influenced Strombolian eruptions of a small-volume parasitic cone complex on the southern ringplain of Mt. Ruapehu, New Zealand: Facies architecture and eruption mechanisms of the Ohakune Volcanic complex controlled by an unstable fissure eruption. J. Volcanol. Geotherm. Res. 327, 99–115.
Kshirsagar, P., Siebe, C., Guilbaud, M.N., Salinas, S., Layer, P.W., 2015. Late Pleistocene Alberca de Guadalupe maar volcano (Zacapu basin, Michoacán): Stratigraphy, tectonic setting, and paleo-hydrogeological environment. J. Volcanol. Geotherm. Res. 304, 214–236.
Kshirsagar, P., Siebe, C., Guilbaud, M.N., Salinas, S., 2016. Geological and environmental controls on the change of eruptive style (phreatomagmatic to Strombolian-effusive) of Late Pleistocene El Caracol tuff cone and its comparison with djacent volcanoes around the Zacapu basin (Michoacán, México). J. Volcanol. Geotherm. Res. 2016, 114–133.
Leonard, G.S., Calvert, A.T., Hopkins, J.L., Wilson, C.J.N., Smid, E.R., Lindsay, J., Champion, D.E., 2017. High-precision $^{40}Ar/^{39}Ar$ dating of Quaternary basalts from Auckland Volcanic Field, New Zealand, with implications for eruption rates and paleomagnetic correlations. J. Volcanol. Geotherm. Res. 343, 60–74.
LGGA, 1925. Crown_583_1925_32. Local Government Geospatial Alliance (LGGA).
Lindsay, J.M., Leonard, G.S., Smid, E.R., Hayward, B.W., 2011. Age of the Auckland Volcanic Field: a review of existing data. N. Z. J. Geol. Geophys. 379–401.
Lorenz, V., 1986. On the growth of maars and diatremes and its relevance to the formation of tuff rings. Bull. Volcanol. 48, 265–274.
McGee, L.E., Millet, M., Smith, I.E.M., Németh, K., Lindsay, J.M., 2012. The inception and progression of melting in a monogenetic eruption: Motukorea Volcano, the Auckland Volcanic Field, New Zealand. Lithos 155, 360–374.
McGee, L.E., Smith, I.E.M., Millet, M., Handley, H., Lindsay, J.M., 2013. Asthenospheric control of melting processes in a monogenetic basaltic system: a case study of the Auckland Volcanic Field, New Zealand. J. Petrol. 54, 2125–2153.
Mochizuki, N., Tsunakawa, H., Shibuya, H., Tagami, T., Ozawa, A., Cassidy, J., Smith, I.E.M., 2004. K-Ar ages of the Auckland geomagnetic excursions. Earth Planets Space 56, 283–288.
Murcia, H., Németh, K., El-Masry, N.N., Lindsay, J., Moufti, M.R.H., Wameyo, P., Cronin, S.J., Smith, I.E.M., Kereszturi, G., 2015. The Al-Du'aythah volcanic cones, Al-Madinah City: implications for volcanic hazards in northern Harrat Rahat, Kingdom of Saudi Arabia. Bull. Volcanol. 77, 1–19.
Needham, A.J., Lindsay, J.M., Smith, I.E.M., Augustinus, P., Shane, P.A., 2011. Sequential eruption of alkaline and sub-alkaline magmas from a small monogenetic volcano in the Auckland Volcanic Field, New Zealand. J. Volcanol. Geotherm. Res. 126–142.
Németh, K., 2010. Monogenetic volcanic fields: Origin, sedimentary record, and relationship with polygenetic volcanism. In: AMERICA, T. G. S. O (Ed.), What is a Volcano?.
Németh, K., Kereszturi, G., 2015. Monogenetic volcanism: personal views and discussion. Int. J. Earth Sci. 104, 2131–2146.
Németh, K., Kósik, S., 2020. Review of explosive hydrovolcanism. Geosciences 10, 44.
Németh, K., Cronin, S.J., Smith, I.E.M., Agustín-Flores, J., 2012. Amplified hazard of small-volume monogenetic eruptions due to environmental controls, Orakei Basin, Auckland Volcanic Field, New Zealand. Bull. Volcanol. 2121–2137.
Németh, K., Gravis, I., Németh, B., 2021. Dilemma of Geoconservation of Monogenetic Volcanic Sites under Fast Urbanization and Infrastructure Developments with special Relevance to the Auckland Volcanic Field, New Zealand. Sustainability 13, 6549.
NZGD, 2016. New Zealand Geotechnical Database. Accessible at: ⟨https://www.nzgd.org.nz/⟩. Ministry of Business Innovation and Employment and the Earthquake Commission, New Zealand.
Ort, M.H., 2009. Lateral vent migration during phreatomagmatic and magmatic eruptions at Tecuitlapa Maar, east-Central Mexico. J. Volcanol. Geotherm. Res. 181, 67–77.
Parfitt, E.A., 2004. A discussion of the mechanisms of explosive basaltic eruptions. J. Volcanol. Geotherm. Res. 134, 77–107.
Parfitt, E.A., Wilson, L., 1995. Explosive volcanic eruptions-IX. The transition between Hawaiian-style lava fountaining and Strombolian explosive activity. Geophys. J. Int. 121, 226–232.
Pedrazzi, D., Bolós, X., Barde-Cabusson, S., Marti, J., 2016. Reconstructing the eruptive history of a monogenetic volcano through a combination of fieldwork and geophysical surveys: the example of Puig d'Àdri (Garrotxa Volcanic Field). J. Geol. Soc. 176, 875–888.
Peti, L., Augustinus, P.C., 2019. Stratigraphy and sedimentology of the Orakei maar lake sediment sequence (Auckland Volcanic Field, New Zealand). Sci. Drill. 25, 47–56.
Polach, H.A., Chappell, J., Lovering, J., 1969. ANU Radiocarbon date list III. Radiocarbon 11, 245–262.
Rout, D.J., Cassidy, J., Locke, C.A., Smith, I.E.M., 1993. Geophysical evidence for temporal and structural relationships within the monogenetic basalt volcanoes of the Auckland volcanic field, New Zealand. J. Volcanol. Geotherm. Res. 57, 71–83.
Schmid, R., 1981. Descriptive nomenclature and classification of pyroclastic deposits and fragments. Int. J. Earth Sci. 70, 794–799.
Searle, E.J., 1959. The Volcanoes of Ihumato and Mangere, Auckland. N. Z. J. Geol. Geophys. 870–888.
Searle, E.J., 1961. Volcanoes of the Otahuhu-Manurewa district, Auckland. N. Z. J. Geol. Geophys. 4, 239–255.
Sigurdsson, H., 2015. The Encyclopedia of Volcanoes. Elsevier, USA.

Smith, I.E.M., Cronin, S., 2021. Geochemical patterns of late Cenozoic intraplate basaltic volcanism in northern New Zealand and their relationship to the behaviour of the mantle. N. Z. J. Geol. Geophys. 64, 201–212.
Sohn, Y.K., Chough, S.K., 1989. Depositional processes of the Suwolbong tuff ring, Cheju Island (Korea). Sedimentology 36, 837–855.
Sohn, Y.K., Park, K.H., 2005. Composite tuff ring/cone complexes in Jeju Island, Korea: possible consequences of substrate collapse and vent migration. J. Volcanol. Geotherm. Res. 141, 157–175.
Sohn, Y.K., Cronin, S., Brenna, M., Smith, I.E.M., Németh, K., White, J.D.L., Murtagh, R. M., Jeon, Y.M., Kwon, C.W., 2012. Ilchulbong tuff cone, Jeju Island, Korea, revisited: a compound monogenetic volcano involving multiple magma pulses, shifting vents, and discrete eruptive phases. GSA Bull. 124, 259–274.
Stats, N.Z., 2018. In: ZEALAND, S. N (Ed.), Auckland Region. Stats New Zealand.
Sulpizio, R., Dellino, P., Doronzo, D.M., Sarocchi, D., 2014. Pyroclastic density currents: state of the art and perspectives. J. Volcanol. Geotherm. Res. 283, 36–65.
Ureta, G., Németh, K., Aguilera, G., Zimmer, M., Menzies, A., 2021. A window on mantle-derived magmas within the Central Andes: eruption style transitions at Cerro Overo maar and La Albóndiga lava dome, northern Chile. Bull. Volcanol. 83, 1–22.
Valentine, G.A., Gregg, T.K.P., 2008. Continental basaltic volcanones - Processes and problems. J. Volcanol. Geotherm. Res. 177, 857–873.
Valentine, G.A., White, J.D.L., 2012. Revised conceptual model for maar-diatremes: Subsurface processes, energetics, and eruptive products. Geology 40, 1111–1114.
Valentine, G.A., Graettinger, A.H., Sonder, I., 2014. Explosion depths for phreatomagmatic eruptions. Geophys. Res. Lett. 41, 3045–3051.
van Otterloo, J., Cas, R.A.F., Sheard, M.J., 2013. Eruption processes and deposit characteristics at the monogenetic Mt. Gambier Volcanic complex, SE Australia: implications for alternating magmatic and phreatomagmatic activity. Bull. Volcanol. 75, 1–21.
Venzke, E., 2013. Global Volcanism Program, Auckland Volcanic Field. *Volcanoes of the World*, 14/05/2021 ed. Smithsonian Institution, Washington, DC.
Viljevac, Z., Murphy, G., Smaill, A., Crowcroft, G., Bowden, D., 2002. South Auckland Groundwater, Kaawa Aquifer Recharge Study and Management of the Volcanic and Kaawa Aquifers. Auckland Regional Council, Technical Publication, New Zealand.
Volosín, S.M., Risso, C., 2019. El Pozo Volcanic complex: Evolution of a group of maars, Central Mendoza province, Argentina. J. Volcanol. Geotherm. Res. 371, 177–191.
Von Veh, M.W., Németh, K., 2009. An assessment of the alignments of vents based on geostatistical analysis in the Auckland Volcanic Field, New Zealand. Géo Morphologie 15, 175–186.
Walker, G.P.L., 1993. Basaltic-volcano systems. Geol. Soc. Lond., Spec. Publ. 76, 3–38.
Waterhouse, B.C., 1966. Mid-tertiary stratigraphy of Silverdale district. N. Z. J. Geol. Geophys. 9, 153–172.
White, J.D.L., Houghton, B.F., 2006. Primary volcaniclastic rocks. Geology 34, 677–680.
Whites Aviation, 1949. Rural property, Papatoetoe, Auckland. In: Alexander Turnbill Library, Wellington, New Zealand: Whites Aviation: Photographs.
Whites Aviation, 1958. Volcanic cone (Wiri Mountain), Manukau City, Auckland Region. In: Alexander Turnbull Library, Wellington, New Zealand: Whites Aviation Ltd: Photographs.
Wohletz, K.H., Sheridan, M.F., 1983. Hydrovolcanic explosions II. Evolution of basaltic tuff rings and tuff cones. Am. J. Sci. 283, 385–413.